NAVAL POSTGRADUATE SCHOOL
Monterey, California

THESIS

30 MeV ELECTRON BEAM IRRADIATION EFFECTS
ON $GaAs_{1-x}P_x$ LEDs

by

James Kevin Foley

June 1985

Thesis Advisor: K. C. Dimiduk

Approved for public release; distribution is unlimited

REPORT DOCUMENTATION PAGE

READ INSTRUCTIONS BEFORE COMPLETING FORM

1. REPORT NUMBER
2. GOVT ACCESSION NO.
3. RECIPIENT'S CATALOG NUMBER

4. TITLE (and Subtitle)
30 MeV Electron Beam Irradiation Effects on $GaAs_{1-x}P_x$ LEDs

5. TYPE OF REPORT & PERIOD COVERED
Master's Thesis
June 1985

6. PERFORMING ORG. REPORT NUMBER

7. AUTHOR(s)
James Kevin Foley

8. CONTRACT OR GRANT NUMBER(s)

9. PERFORMING ORGANIZATION NAME AND ADDRESS
Naval Postgraduate School
Monterey, California 93943-5100

10. PROGRAM ELEMENT, PROJECT, TASK AREA & WORK UNIT NUMBERS

11. CONTROLLING OFFICE NAME AND ADDRESS
Naval Postgraduate School
Monterey, California 93943-5100

12. REPORT DATE
June 1985

13. NUMBER OF PAGES
97

14. MONITORING AGENCY NAME & ADDRESS (if different from Controlling Office)

15. SECURITY CLASS. (of this report)
UNCLASSIFIED

15a. DECLASSIFICATION/DOWNGRADING SCHEDULE

16. DISTRIBUTION STATEMENT (of this Report)
Approved for Public release; distribution is unlimited

17. DISTRIBUTION STATEMENT (of the abstract entered in Block 20, if different from Report)

18. SUPPLEMENTARY NOTES

19. KEY WORDS (Continue on reverse side if necessary and identify by block number)
LEDs, $GaAs_{1-x}P_x$, electron beam, Bremsstrahlung losses, electroluminescence, damage constant

20. ABSTRACT (Continue on reverse side if necessary and identify by block number)
LEDs of the ternary alloy $GaAs_{.7}P_{.3}$, were irradiated with a 30 MeV electron beam. The effects this exposure had on peak wavelength, absolute and relative light output intensities, and current-forward bias characteristics were studied. A simple model of LED current controlling mechanisms is described and a mathematical approach for deriving a descriptive damage-constant is provided. Observed irradiation effects consisted of increased current and decreased light output intensity for a given forward bias voltage and indicate that the devices tested are an order of magnitude softer (con't)

to electron radiation than results previously reported. Damage constants were calculated: group 9 (2.9×10^{-14} cm^2/e), group A5 (2.6×10^{-14} cm^2/e), and group 3 (1.4×10^{-14} cm^2/e). Shielded and un-shielded devices were compared to determine if the secondary electron production for Bremsstrahlung losses would reduce the total fluence required for degradation. The results of this experiment were inconclusive. A procedure was developed to determine the electron beam current density for use in dose estimations. Electron doses were a factor of three higher when compared to the previous method of calculation.

Approved for public release; distribution is unlimited

30 MeV Electron Beam Irradiation Effects on $GaAs_{1-x}P_x$ LEDs

by

James Kevin Foley
Lieutenant, United States Navy
B.S., United States Naval Academy, 1978

Submitted in partial fulfillment of the
requirements for the degree of

MASTER OF SCIENCE IN PHYSICS

from the

NAVAL POSTGRADUATE SCHOOL
June 1985

ABSTRACT

LEDs of the ternary alloy $GaAs_{.7}P_{.3}$ were irradiated with a 30 MeV electron beam. The effects this exposure had on peak wavelength, absolute and relative light output intensities, and current-forward bias characteristics were studied. A simple model of LED current controlling mechanisms is described and a mathematical approach for deriving a descriptive damage-constant is provided. Observed irradiation effects consisted of increased current and decreased light output intensity for a given forward bias voltage and indicate that the devices tested are an order of magnitude softer to electron radiation than results previously reported. Damage constants were calculated: group 9 (2.9×10^{-14} cm^2/e), group A5 (2.6×10^{-14} cm^2/e), and group 3 (1.4×10^{-14} cm^2/e). Shielded and un-shielded devices were compared to determine if the secondary electron production from Bremsstrahlung losses would reduce the total fluence required for degradation. The results of this experiment were inconclusive. A procedure was developed to determine the electron beam current density for use in dose estimations. Electron doses were a factor of three higher when compared to the previous method of calculation.

TABLE OF CONTENTS

ACKNOWLEDGEMENT

Prof. Kathryn Dimiduk deserves much of the credit for the completion of this work. As my advisor, her recommendations concerning the research and the vigilance she exhibited in reviewing my work is greatly appreciated.

I would also like to thank Prof. K. Woehler for his patience and insight into the beam cross-section experimental results. His data interpretation was of great help in resolving the final derivation. Thanks also go out to Prof. X. Maruyama, whose undiminished enthusiasm for working in and around the LINAC helped me through the dark times. Don Snyder's expertise at the Linac control station was of invaluable help. His friendly demeanor and helpful attitude will always be appreciated.

Finally, I would like to thank Mr. S. Hall of the Optoelectronics Division of Hewlett-Packard for providing the LEDs used in the research.

I. INTRODUCTION

A. OVERVIEW

In recent years, applications for solid-state semiconductors have grown dramatically. Specifically, devices utilizing the electroluminescence properties of III-V compound semiconductor alloys in producing efficient, cheap light emitting diodes (LED) have seen remarkable progress. In light of the fact that many of these devices can and will serve as integral parts to many military systems, the question as to how effective these devices will remain after exposure to ionizing radiation, such as might be experienced after a nuclear attack or in an outer space environment, becomes a pertinent one.

$GaAs_{1-x}P_x$ (Gallium-Arsenide-Phosphide) is one such type of III-V compound that is popular in the field of LED fabrication. Common modes of employment are in optical displays, opto-isolators, and optical encoders.

Light Emitting Diodes (LEDs) are characterized by the fact that under the proper forward-biased conditions, they can emit external spontaneous radiation in selected wavelengths which span the electromagnetic spectrum from blue to the infrared. Basically, the mechanism that is responsible for the optical emission is called

recombination. An injected electron or hole recombines with (i.e. annihilates) a particle of the opposite type and in the process, gives off energy. This energy can be in the form of photons (light) or phonons (heat). The process in which photons are the product of the recombination is termed a "radiative recombination". However, if phonons are the result, a "non-radiative recombination" has resulted and these will detract from the efficiency of the LED by stealing electron/hole pairs away from the desired radiative centers.

In this research, radiation effects on $GaAs_{.7}P_{.3}$ LEDs were studied. The devices used were supplied by Hewlett Packard Optoelectronics Division of Palo Alto, California, and their intended uses are as optical isolators and encoders. The LEDs were supplied in a modified TO-46 can of Covar alloy and not in the packaging or configuration used for commercial marketing. This allowed the research efforts to be concentrated on the semiconductor chip itself without the interference that superfluous packaging might present. A complete characterization of the devices can be found in Chapter III.

Although radiation products from a nuclear explosion can vary from high energy gamma rays, neutron, and x-rays to beta rays (i.e. electrons), this research focused its attention on the effect that medium energy (30 MeV) electrons had on the LED's operating characteristics.

Voltage versus current data as well as optical output intensity where taken both prior to and after electron irradiation. The Naval Postgraduate School's Accelerator Laboratory (NPSAL), which contains a linear accelerator capable of producing 110 MeV electrons, provided the 30 Mev electrons used for the research. Details of the experimental set up and the NPSAL linear accelerator operation can be found in Chapter III.

B. PREVIOUS RESEARCH

Stanley [Ref. 1] examined the effect of 2 to 2.5 MeV electron irradiation on $GaAs_{1-x}P_x$ LEDs and found that their conversion efficiencies were reduced by the ionizing radiation generating additional recombination centers for non-radiative transitions.

Barnes [Ref. 2] gives a good overview of the theory and operations of LEDs. He also surmises that if the light intensity of the LED is due to recombination in the neutral region (i.e. diffusion controlled), the total light intensity will depend on the minority carrier lifetime. He further states that if the assumption is made that radiation induced damage take the form of non-radiative recombination centers in the matrix, the light intensity of the LED will decrease at a constant voltage as the lifetime decreases due to irradiation. Barnes also found that in terms of resistance to radiation induced defects, the hardness of the

devices were inversely proportional to their purity and quality.

Aukerman and Millea [Refs. 3 thru 6] accomplished an indepth study of electron irradiation effects and described the proposed mechanisms causing the resultant bulk damage effects.

Schade et al. [Ref. 7] irradiated $GaAs_{1-x}P_x$ LEDs with a 1 Mev electron beam. Their work showed that the light output of the LEDs did indeed diminish with increased electron fluence and could be attributed to two different types of non-radiative defect centers that were directly attributable to bombardment by the electron beam. The center thought to be primarily responsible for the decrease in light emission was an acceptor site with concentrations on the order of 1 to 5 x $10^{17}cm^{-3}$ and whose influence was generally independent of alloy composition. The second type was trapping centers located 0.20 to 0.33 eV from either band edge. Unlike the acceptor sites, the concentrations of the trapping centers were found to increase with alloy composition (i.e. increasing x).

Rose and Barnes [Ref. 8] studied the effect of a comparatively high energy proton beam, 16 MeV, irradiation of the devices. The theory they presented for analyzing their results is the basis for damage constant calculations in the following Chapters.

C. ORGANIZATION OF PRESENT WORK

The remainder of the work will be organized as follow. Chapter II presents a brief review of the theory of operation of semiconductors and light emitting diodes. Temperature dependencies will be discussed and a section concerning electron radiation effects on matter are included. A scheme to catagorize damage effects on the LEDs completes the chapter. Chapter III describes the experimental procedures and includes a detailed description of work done to characterize the electron beam profile of the NPSAL LINAC beam. Chapter IV presents the results of the research which includes comparisons with other pertinent works. Chapter V contains conclusion of this research and recommendations for future work in this area.

II. THEORETICAL BACKGROUND

A simplified model is presented of light emitting diode (LED) operation which includes an examination of current flow and luminescence mechanisms. Effects of electron irradiation on matter and specifically semiconductors is addressed and a scheme for characterization of damage to LEDs through the use of a damage constant is developed.

A. LIGHT EMITTING DIODE OPERATIONS

Within the much broader heading of semiconductors, there exists a small subset of devices known as light emitting diodes or LEDs. These diodes are important because of their ability to undergo electroluminescence. Electroluminescence is the generation of light by an electric current passing through a material under an applied electric field. Of specific concern here is injection electroluminescence or optical radiation obtained by injection of minority carriers into the region of a semiconductor's p-n junction were radiative transitions take place.

1. Current Flow Mechanisms

In the simplest steady-state model of an LED, electrons are induced to flow through the material by the process of thermal excitation. When an external electric field is present, other processes such as diffusion or space

charge recombination can become dominant and control the characteristic behavior of the diode. These various current flow mechanisms are discussed in the following subsections.

a. Thermally Induced Current

According to the principles of Statistical Mechanics, electrons and holes possess the thermal energies associated with a classical free particle:

$$\frac{1}{2} m^* v_{th}^2 = \frac{3}{2} kT \qquad (1)$$

where m^* is the effective mass of the free electron in a given material, k is the Boltzman constant, and T is the absolute temperature in degrees Kelvin. At a given temperature, the electrons can be pictured as randomly moving about within the lattice, undergoing numerous collision between themselves and the lattice. The higher the temperature, the faster and more violently the electrons move about and, consequently, collisions are more numerous. At thermal equilibrium, the net current flow is effectively zero due the statistical interpretation that as any number of electrons move in one direction, an equal number move in the exact opposite direction.

b. Drift Current

In addition to undergoing these thermally induced random collisions, if an externally applied electric field is present, the electrons are accelerated along the direction of the field lines. The net carrier velocity in the presence of an applied electric field is termed the drift velocity, v_d. Muller and Kamins [Ref. 9] state that the drift velocity can be found by equating the impulse applied to the electron by the electric field during its free flight between collisions to the momentum gained during the same time period. Therefore, expressing impulse as force multiplied by time gives

$$-qE\tau_c = m^*v_d \tag{2}$$

where E is the magnitude of the electric field and τ_c is the mean scattering time between collisions. The minus sign indicates the negative charge possessed by the electron. Solving for the drift velocity yields

$$v_d = \frac{-qE\tau_c}{m^*} \tag{3}$$

The collection of terms

$$\mu_n = \frac{q \tau_c}{m^*} \tag{4}$$

is referred to as the mobility of the free electron and describes how strongly the electron's motion is influenced by an external electric field. The drift current can be found from the product of the charge on each electron and its drift velocity or

$$I = -qV_d = q\mu_n E \tag{5}$$

This type of current mechanism closely approximates ohmic behavior.

c. Diffusion Current

Unlike metals, semiconductors possess a current component that is due to spatial variations of carrier densities and is termed the diffusion current. As with any diffusion phenomenon, the carriers tend to flow from a region of high density to lower densities. If the semiconductor is not under any applied bias, the carriers undergo random thermal motions as discussed previously. However, these random motions have a net direction which is

along the density gradient. Consider the net flux measured in units of particles per unit area per unit time across an arbitrary plane within the semiconductor material. This can be expressed as

$$FLUX = -v_{th} l \Delta n \tag{6}$$

where Δn is the density gradient in one dimension and l is the mean free path between collisions for the particle. The mean free path is equal to

$$l = v_{th} \tau_c \tag{7}$$

Therefore, if we consider the particles to be electrons, the diffusion current density can be expressed as

$$J = -q \cdot FLUX = q v_{th} l \Delta n \tag{8}$$

Using the equipartition of energy theorm in one dimension (similar to equation. 1) along with Equations (4) and (7),

the diffusion current in equation (8) can now be expressed as

$$J = q D_n \Delta n \tag{9}$$

This new constant D_n is known as the diffusion constant and is equal to

$$D_n = \frac{kT}{q} \mu_n \tag{10}$$

Equation (10) is known as the Einstein Relationship [Ref. 10] and expresses the relationship that exists between the diffusion constant (which characterizes diffusion transport mechanisms) and the mobility (which characterizes drift transport mechanisms). Note the temperature dependence.

d. Ideal Diode Equation

Thus far we have described the conditions within a single-type material, that is p or n. Muller and Kamins [Ref. 9] present an excellent outline for the development of the ideal diode equation. This equation is used to express the current caused by the flow of injected minority carriers

into the depletion region. The equation is presented below without proof

$$J_t = J_o[\exp(qV_a/kT) - 1] \qquad (11)$$

J_t represents the total current density which is the sum of drift and diffusion currents, V_a is the applied bias, and J_o is the saturation current density produced in the presence of a negative bias of a few kT/q volts. In ternary alloys such as $GaAs_{1-x}P_x$, results based on the ideal diode equation only qualitatively agree with the actual current-voltage characteristics [Ref. 10]. A source of the disagreement lies in the failure of the ideal diode equation's assumption that electron and hole current is constant throughout the depletion region [Ref. 11]

e. Space-Charge Recombination Currents

In view of the failure of the ideal diode equation to properly explain the current-voltage characteristics within the space-charge region, another mechanism has been suggested to better approximate experimental results. Sze [Ref. 10] states that under forward bias, within the space-charge region, the major recombination-generation processes are the capture processes. Therefore, there exists a recombination current that varies exponentially with the applied forward bias

voltage in addition to the diffusion current. These space-charge recombination currents have been found to contribute to the saturation current in magnitudes comparable to the diffusion currents [Ref. 11].

Experiments have shown that, in general, the total current for forward bias can be approximated by the expression

$$I_F \approx I_o \exp(qV_a/nkT) \qquad (12)$$

where the factor n = 2 when space-charge recombination current is dominant and n = 1 when diffusion current is dominant. [Ref. 11]

2. Electroluminescence Phenomenon

As stated previously, the electroluminescence phenomenon is caused by the recombination of the injected electrons or holes by a carrier of the opposite type. However, recombinations can be of two different kinds: radiative on non-radiative. Only the radiative recombinations result in the release of energy in the form of photons (light). Recombinations of the non-radiative type result in the release of energy in the form of phonons or heat.

a. Direct and Indirect Recombinations

Figure 1 depicts the possible recombinations

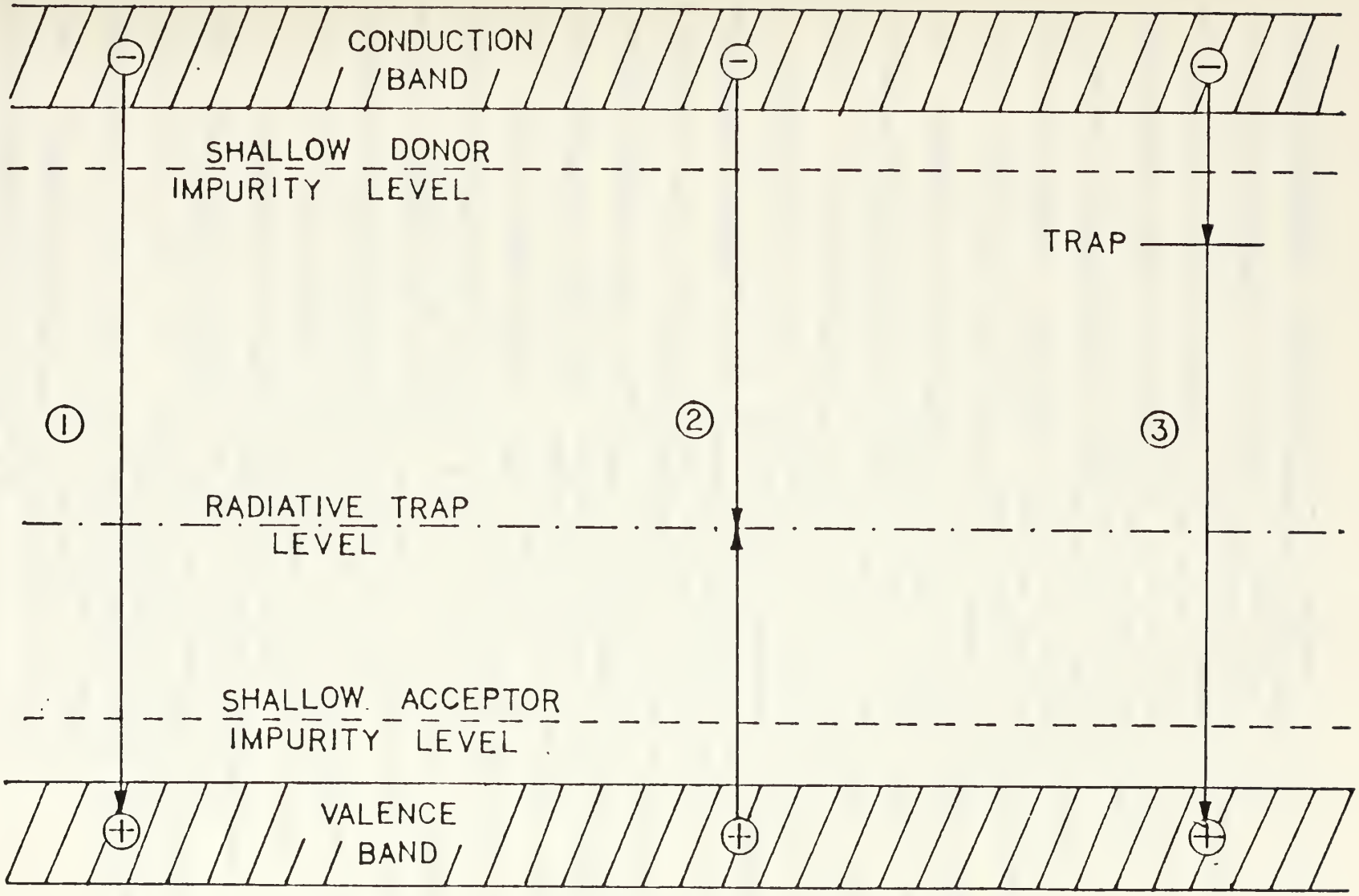

Figure 1. Possible Recombination Mechanisms in a Semiconductor

available in a representative semiconductor. Transition 1 is a direct band-to-band recombination of an electron in the conduction band with a hole in the valence band. The photon energy released will be on the order of the band gap energy of the material itself. This process predominates in direct gap semiconductors such as GaAs. Transition 2 depicts the indirect method of radiative recombinations. Specific impurities or defects, when introduced into the crystal lattice, can result in the formation of specialized center or trap located within the forbidden zone of the semiconductor. Recombination centers formed in this manner are most often electrically neutral. As an example, consider in a p-type material, an injected electron is first trapped at the neutral recombination center. No longer neutral due to the electron's negative charge, the center attracts a hole from the valence band to form a bound exciton. The subsequent annihilation of this electron-hole pair emits a photon whose energy is equal to the band gap energy minus the binding energy of the specialized recombination center. This type of radiative recombination predominates in indirect band-gap materials such as GaP. Transition 3 depicts the non-radiative type of recombinations that results in phonon energy release.

b. Ternary Compounds

Ternary compounds such as $GaAs_{1-x}P_x$ have the distinction that they can exhibit the characteristics of

direct or indirect band gap materials depending on the mole fraction of the alloy, indicated by the value of the subscript x. Figure 2 shows a plot of the conduction band edge and the valence band edge as a function of momentum versus band gap energy for different alloy compositions. As shown, there exist two minima within the conduction band, one designated direct and the other indirect. Electrons existing in the direct minimum of the conduction band and holes at the top of the valence band possess the same momenta, whereas electrons in the indirect minimum do not. In consideration of the conservation of momentum, there exists a high probability for band to band transitions for electrons in the direct minimum. For electrons in the indirect minimum, the probability of transition is close to zero because an additional component (phonon) must interact for momentum conservation to be observed. This is why indirect band gap materials require the introduction of special recombination centers within the lattice to enhance the radiative recombination process. GaAs and $GaAs_{1-x}P_x$ with x approximately equal to or less than 0.4 act as direct band gap materials whereas $GaAs_{1-x}P_x$ with $x > 0.4$ and GaP act as indirect band gap materials [Ref. 12]. Figure 3 shows the compositional dependence of the direct and indirect energy band gap for $GaAs_{1-x}P_x$. Note that the band gap energy increases with increasing mole fraction x.

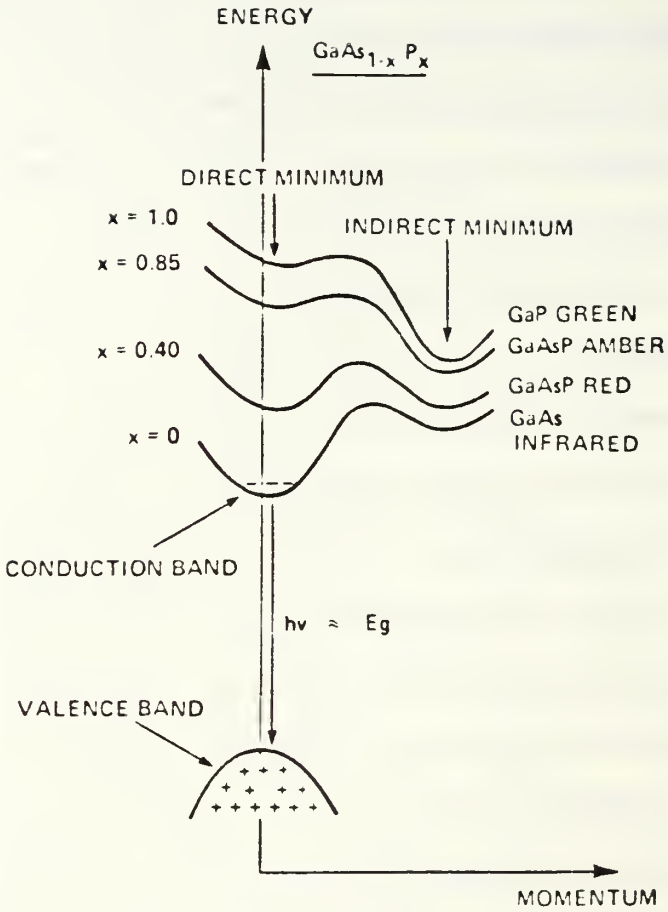

x	E_D eV	E_I eV	λ (nm)
0.	1.43	1.86	910
0.40	1.92	1.97	650
0.85	1.55	2.17	580
1.0	2.78	2.26	560

Figure 2. Conduction and Valence Band Edges as Functions of Momenta for $GaAs_{1-x}P_x$ [Ref. 12, p. 1.3]

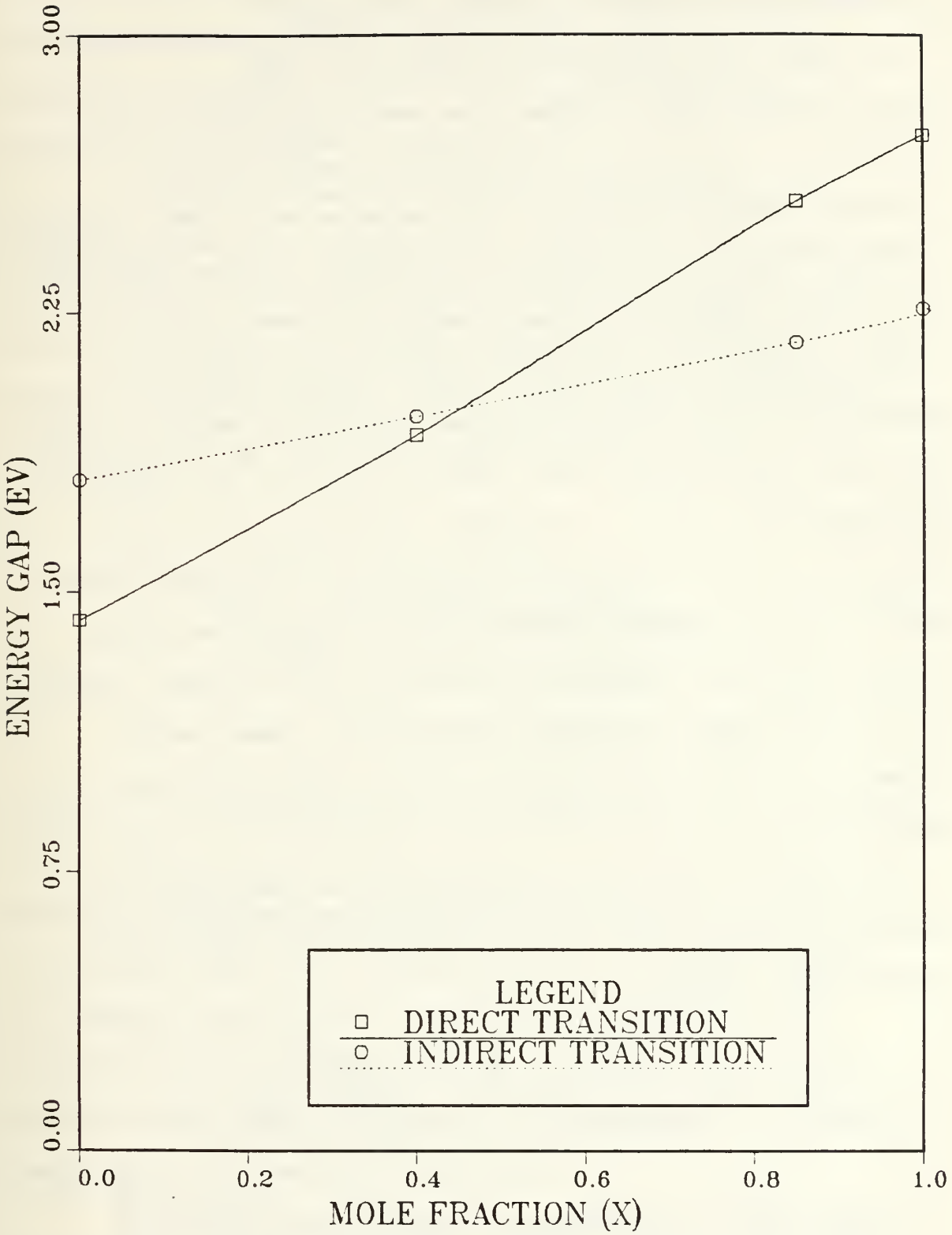

Figure 3. Compositional Dependencies for Direct and Indirect Band Gap Energies in $GaAs_{1-x}P_x$

B. RADIATION EFFECTS OF ELECTRONS IN MATTER

Now that the processes of current flow and electroluminescence in LEDs have been described, it is important to discuss how radiation can affect their characteristics. Electrons, when compared with heavy charged particles (e.g. alpha particles, protons), can be described as having a tendency to lose energy at a lower rate and follow a much more complicated path through absorbing materials. These large deviations are due, in part, to the electron's mass being nearly equal to that of the orbiting electrons with which it interacts (ignoring relativistic effects). An additional consideration is that a much larger portion of the electron's energy can be lost in a single interaction and a possibility exists of the electron losing all of its energy during one interaction. These energy losses can occur through collisions or radiative loss mechanisms.

Enge [Ref. 13] gives an expression that describes an electron's energy loss due to ionization and excitation (collisional losses)

$$\left(-\frac{dT}{dX}\right)_i = \frac{e^4 NZ}{8\pi\epsilon_0^2 m_0 v^2}\left[\ln\frac{m_0 v^2 T}{2I^2(1-\beta^2)} - \left(2\sqrt{1-\beta^2}-1+\beta^2\right)\ln 2 + 1 - \beta^2 + \frac{1}{8}\left(1-\sqrt{1-\beta^2}\right)^2\right] \quad (13)$$

where Z is the atomic number (i.e. the number of protons) of the absorbing material, T is the kinetic energy of the electrons, and β is the ratio of the velocity of the electrons to the speed of light (v/c).

Radiative losses in electrons take the form of Bremsstrahlung or electromagnetic radiation. This occurs as the electron is subjected to an acceleration within the field of the nucleus or another electron in accordance with classical electromagnetic theory. Rudie [Ref. 14] presents an expression for radiative stopping power as

$$\left.\frac{dT}{dX}\right|_{rad} = N\left(T + m_o c^2\right)\sigma_{rad} \qquad (14)$$

where σ_{rad} is the radiative cross section and is a function of the square of the atomic number of the absorbing material. By comparing equations (13) and (14), it becomes evident that collision losses dominate within the region of low electron energies and, conversely, higher electron energies lead to the dominance of radiative losses. The regions of dominance are necessarily dependent on the atomic number (Z) of the absorbing material.

Rudie [Ref. 14] gives an equation for a "critical energy" as

$$T_C = \frac{800}{1.2 + Z} \text{ MeV} \qquad (15)$$

This critical energy marks a line of demarcation between the predominance of radiative losses and collision losses. If a Z for Ga or As is used in equation (15), T_C is equal to 25 MeV which is less than the average beam energy (30 Mev) used for this research. This would indicate that radiative losses should dominate.

Although a preponderance of the prior research has stated that the primary mechanism for radiation-induced damage in semiconductors has been the introduction of displacements within the crystal lattice caused by the electrons undergoing collisional losses, the results of Equation (15) raises some questions. Experiments detailed in Chapter III describe irradiation runs done on LEDs that had their Covar cans removed. The results of these runs were compared to results from irradiation of LEDs that had their can left on to see if their was a noticeable difference in the amount of electron fluence required for degradation. It was thought that as the beam traversed the can, the radiative loss mechanism would be enhanced causing a shower of secondary electrons. These secondary electrons, in addition to the electrons in the main beam, would cause the

degradation. However, the details of these damage interactions were not investigated. Only the differences in the amounts of fluence required for degradation between the groups with their cans removed and their cans remaining was studied.

Changes in the current-voltage characteristics after irradiation are important parameters in describing damage done to the LEDs. Through the use of a phenomenological theory, these changes can be described in terms of a damage constant.

2.Damage Constant Development

One way of describing the efficiency of an LED is based on the number of injected minority carriers that undergo radiative recombinations as compared to the number that undergo non-radiative recombinations. Rose and Barnes [Ref. 8] stated that exposure to radiation introduces dislocations or displacements within the orderly crystal lattice. These defects tend to act as traps or non-radiative recombination centers that compete with the radiative recombination centers for the injected carriers. This competition results in a decrease of the injected carriers' lifetime and, therefore, an overall degradation of emitted light.

Rose and Barnes outline a phenomenological method for determining a damage constant as follows. The total initial

lifetime of the injected minority carriers can be expressed as

$$\frac{1}{\tau_0} = \frac{1}{\tau_{0r}} + \frac{1}{\tau_{0_{nr}}} \qquad (16)$$

where τ_0 is the total pre-irradiation minority carrier lifetime, and τ_{0r} and $\tau_{0_{nr}}$ are lifetimes associated with radiative and non-radiative processes. These can be further expressed as

$$\frac{1}{\tau_{0_r}} = \sigma_r v_{th} N_r \qquad (17)$$

and

$$\frac{1}{\tau_{0_{nr}}} = \sigma_{nr} v_{th} N_{nr} \qquad (18)$$

where σ_r and σ_{nr} are carrier capture cross-sections associated with radiative and non-radiative centers respectively. N_R and N_{NR} are the concentrations of radiative and non-radiative centers.

After irradiation, the total injected minority carrier lifetime is expressed as

$$\frac{1}{\tau} = \frac{1}{\tau_{o_r}} + \frac{1}{\tau_{o_{nr}}} + \sigma_{nri} v_{th} N_{nri} \qquad (19)$$

or

$$\frac{1}{\tau} = \frac{1}{\tau_o} + \sigma_{nri} v_{th} N_{nri} \qquad (20)$$

The additional term in equation (19) is a product of the radiation induced non-light-producing centers. The usual procedure is to define the concentration of these radiation induced centers by

$$N_{nri} \equiv C_1 \phi \qquad (21)$$

where ϕ is the radiation fluence and C_1 is a constant whose magnitude involves the probability of generation of defects by a unit radiation fluence. If the damage constant K is defined by

$$K \equiv \sigma_{nri} v_{th} C_1 \qquad (22)$$

then the equation used to describe LED radiation damage is given by

$$\frac{1}{\tau} = \frac{1}{\tau_0} + K\phi \tag{23}$$

or

$$\frac{\tau_0}{\tau} = 1 + \tau_0 K\phi \tag{24}$$

Although the physics involved in describing the interactions of radiation with the semiconductor material is contained within the damage constant K, this phenominological approach for degradation predictions is useful. In view of this fact, $\tau_0 K$, the value of the initial lifetime damage constant product, becomes the quantity of prime interest.

If τ and τ_0 could be measured, K could be derived directly through Equation (24). However, light output intensity is much easier to measure. Therefore, part of the data that was gathered during the course of this research was the LED current and light output as a function of forward bias, both pre and post irradiation. Having this data in graphical form allowed the determination of the slope of the I vs V curves. This slope could then be used in

Equation (12) to determine the current controlling mechanism for the devices under study. Equipped with this, a useful damage constant tailored for the environment that the device operates in can be developed. As an example, if the device under study has radiative current that is diffusion controlled, an expression can be given that relates the light output to the injected minority carrier lifetime by

$$L = C\tau \exp\left(\frac{qV_a}{kT}\right) \tag{25}$$

where C is a constant containing parameters that are independent of τ or T. Using this relationship in equation (24), under the device operating condition of constant voltage , it can be shown that

$$\frac{\tau_0}{\tau} = \frac{L_0}{L} = 1 + \tau_0 K \phi \tag{26}$$

where L_0 and L are pre-irradiation and post irradiation light output respectively. The procedures employed in gathering this data and considerations concerning the data gathering environment are presented in Chapter III.

III. EXPERIMENTAL PROCEDURES

This chapter provides a physical description of the operating characteristics of the light emitting diodes used in this research along with experimental procedures and considerations. Operating parameters of the NPSAL LINAC are listed and a discussion concerning the determination of the cross-sectional profile of the electron beam is presented.

A. PHYSICAL CHARACTERISTICS OF EXPERIMENTAL LEDS

The light emitting diodes used for this research were supplied by the Optoelectronic Division of the Hewlett-Packard Company located in Palo Alto, California. The diodes are made of a $GaAs_{1-x}P_x$ ternary alloy with the mole fraction $x = 0.3$, which implies that these are direct gap semiconductors. A cross-section and top view of a typical LED is given in Figure 4. The $GaAs_{.7}P_{.3}$ layer was grown on a GaAs substrate by vapor phase epitaxy with the p-n junction lying 1 to 3 microns beneath the surface. Tellurium was used for the n-type dopant with typical concentrations of $3x10^{17}$ electrons/cm^2; Zinc, with concentrations at the junction of 10^{19} holes/cm^2, was the p-type dopant. The junction exhibited an exponential doping profile [Ref. 15].

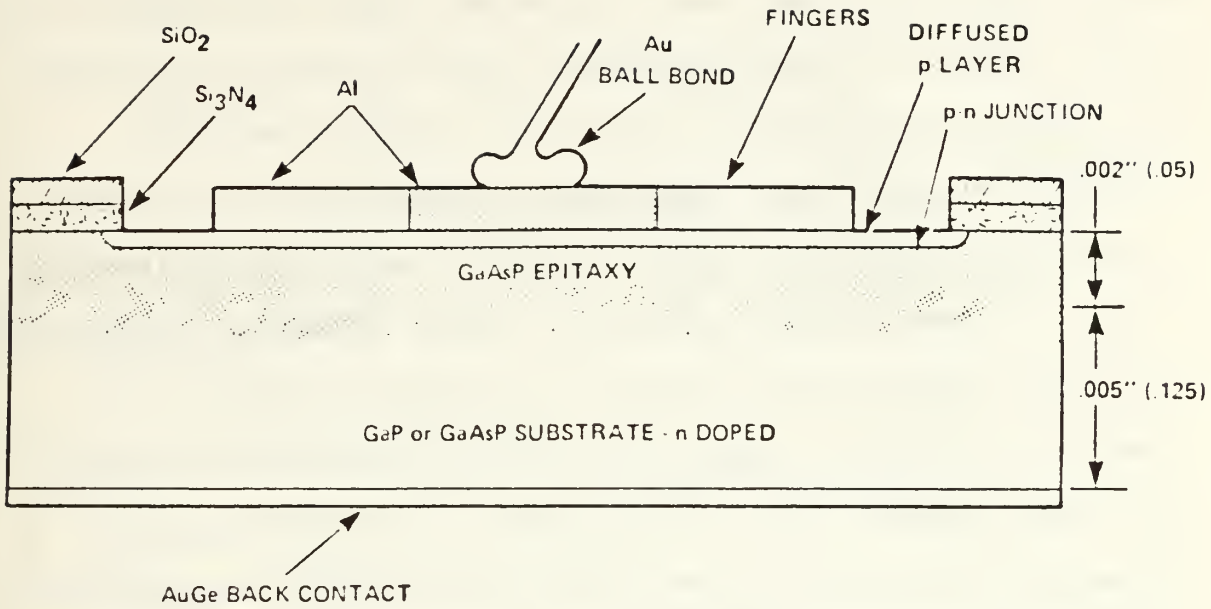

CROSS SECTION OF AN LED

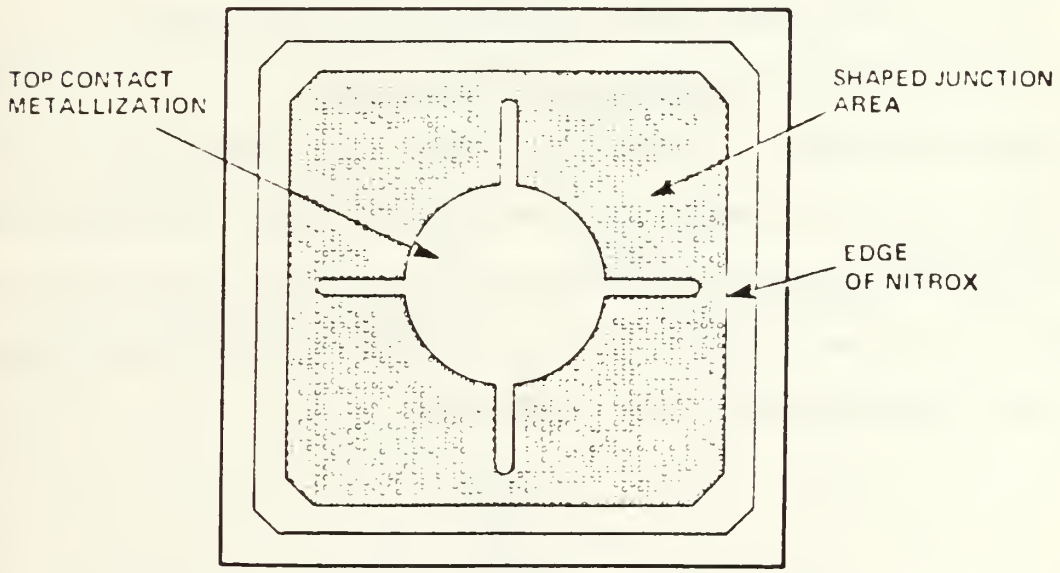

PLAN VIEW OF AN LED

Figure 4. Cross-Sectional and Top View of a Typical LED [Ref. 12, p. 1.7]

The diodes were divided into three groups according to their light emitting area. They were exactly the same in all other respects. Figure 5 depicts the top view of the groups and their corresponding dimensions. Groups 3 and A5, characterized by their rectangular shaped area of emittance, are to be commercially used as optical encoders while group 9 will be used as opto-couplers. A more in-depth description of these devices can be found in the 1985 Optoelectronic Designer's Catalog [Ref. 16]. It is of importance to note that the devices were not supplied in the configuration intended for commercial marketing. Rather, the semiconductor chip was mounted at the base of a Covar can, which was open at the top. No lens or plastic covering was present at the top end and all electrical connections were made through existing wires at the base.

The diodes were first categorized as per their characteristic wavelength. A Beckman DK-1A spectrophotometer, modified to allow the LEDs to act as the light source, was used for the purpose and a wavelength of 720nm was found for all three groups. Sproull and Phillips [Ref. 17] give an equation that relates the band gap energy to the characteristic wavelength as

$$\lambda = \frac{1240}{\Delta E} \text{ nm} \qquad (27)$$

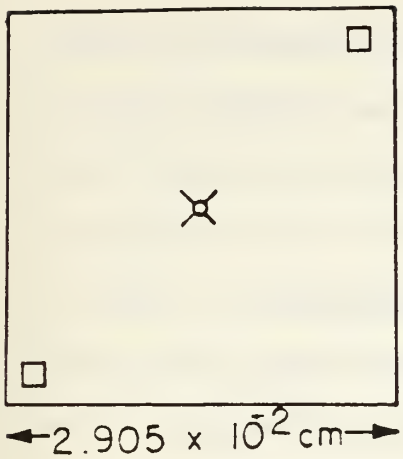

GROUP 3

AREA = 8.44×10^{-4} cm^2

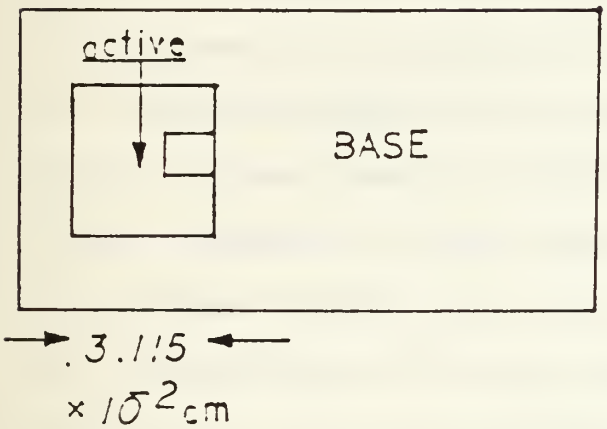

GROUP A5

ACTIVE
AREA = 9.70×10^{-4} cm^2

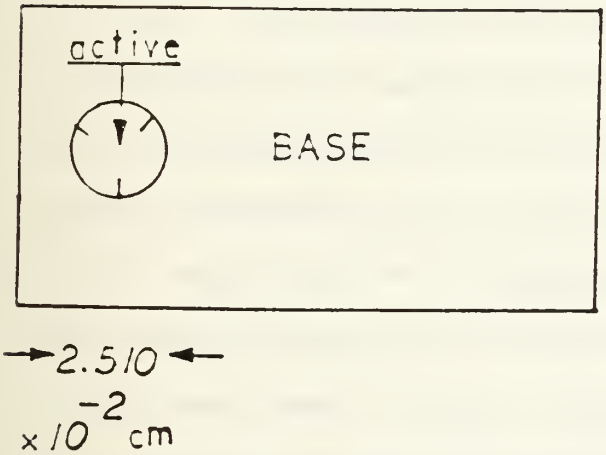

GROUP 9

ACTIVE
AREA = 4.95×10^{-4} cm^2

Figure 5. Top View of Experimental LEDs

After determining that the wavelength of the devices is 720 nm, the band gap energy can be calculated to be 1.72 eV, which is in good agreement with Figure 3 for the mole fraction x = 0.3.

Equation (12) shows the temperature dependence of the forward current to be exponential in nature. Also, in Reference (12), it is stated that the peak wavelength, output power, and luminous intensity all vary with temperature. The peak wavelength increases by 0.2 nm/°C. Radiant power decreases as temperature increases on the order of -1%/°C for direct band gap materials, and the luminous intensity exhibits a logarithmic relationship with temperature. In view of these facts, preliminary testing was done to see if temperature effects would be significant enough to warrant their consideration.

A scheme was developed whereby the environmental temperature of the LEDs could be controlled. An aluminum adapter, used in conjunction with the 550 power meter to hold the LEDs in place during testing, was modified for this purpose. Insulated wire of resistance 11.97 ohm/ft was coiled around the adapter that would be holding the LED. The ends were then attached to a power supply to fabricate a localized heating element. It was found that by controlling the current through the wire an isolated area of constant temperature could be produced and regulated easily. In this manner, the LED could be placed in a "pocket" of desired

temperature and kept there. Teflon tape placed between the aluminum adapter and the case containing the semiconductor sensor head was felt to adequately insulate the sensor from unnecessary heat exposure. A Chromel-Constantan thermocouple attached to the base of the LED was used to monitor the temperature. A series of current versus voltage readings were taken on a randomly picked LED at three constant temperatures, each separated by 10°C, to see if these slight temperature differences would be noticeable. In view of the results depicted in Figure 6, it is felt that the effects of increasing temperature were significant enough to warrant that all further characterizations (except those done during irradiation) be done at constant temperature. 30°C was chosen as it was close to, but above, ambient temperature and therefore easily obtainable.

Light output intensity readings were then taken in conjunction with the current versus forward bias voltage data. Three LEDs from each group were measured, both pre and post irradiation. A circuit consisting of a Hewlett-Packard power supply (model 6216B) in series with a 75 ohm resistor and the LED was used. Voltage and current reading were taken using two Fluke (model 75) multimeters and the output light intensity readings were performed with a Fiber Optic Power Meter (model 550) equipped with a silicon photodiode detector head. The power meter measures the output intensity of the LED and compares it to a calibrated microwatt

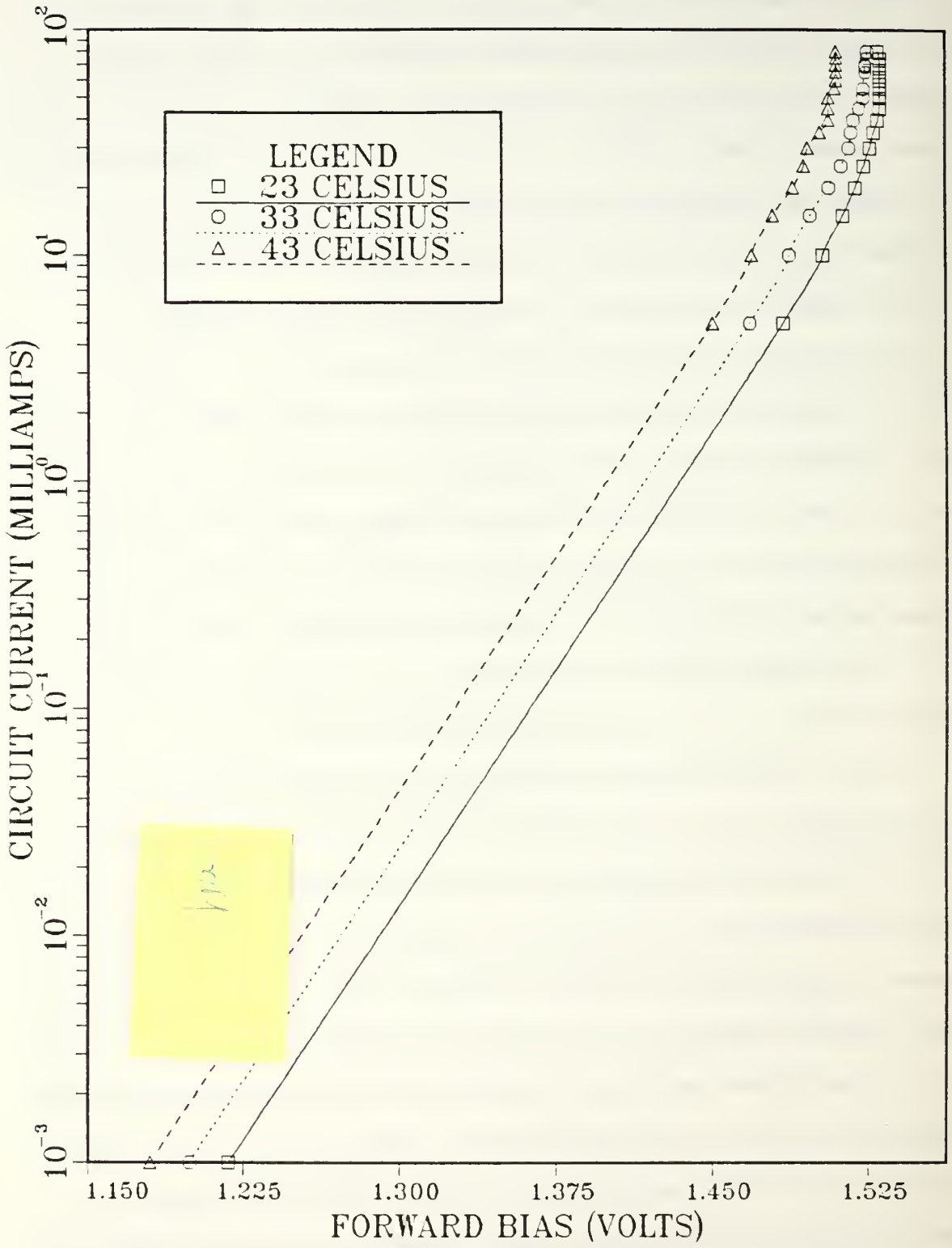

Figure 6. Alteration of Current-Voltage Characteristics due to Varying Temperatures

internal reference. A correction factor based on the characteristic wavelength of the device, must then be added to arrive at the proper power reading (in microwatts) of the specific device being tested. For the devices used in this research, the correction factor added was 0.871 for a characteristic wavelength of 720 nm. The forward bias voltage was slowly increased until an initial current was detected by the Fluke multimeter. Due to the accuracy of the meter, one microamp was the minimum discernible signal and the voltage value at this reading was termed the "turn-on" voltage of the diode. After this value was reached, voltage and output light intensity were taken at intervals of 5mA.

B. IRRADIATION PROCEDURES

The NPSAL LINAC provided the necessary source of accelerated electrons for this research. The LINAC employs an electron gun (i.e. cathodic grid) to initially produce the electron population. After generation, the electrons are accelerated down a wave guide under the influence of RF energy produced by a series of klystrons. The beam is bent 45° off of the acceleration axis by magnets at which point it enters the end station and subsequent target chamber. Focusing of the beam is accomplished by a quadrapole magnet located directly prior to the target chamber. The quadrapole can focus the beam down to a spot

with an approximate radius of 2mm or "defocus" it to resemble a rectangle of area 5 square cm. The spot size used for this research was a rectangle of area 0.52 square cm. This size was felt to be large enough to ensure coverage of the device by the beam.

The NPSAL LINAC is capable of producing a 110MeV beam, however, a 30MeV beam was used for this research. The LINAC operates in a pulsed mode with a pulse repetition rate of 60 pulses per second and an average pulse duration on the order of 2.5×10^{-6} seconds. There is a theoretical peak of 10^{11} electrons per pulse. However, in practice, beam fluence was measured through the use of a Secondary Emissions Monitor (SEM) located at the rear of the target chamber. As the electron beam passed through the SEM, a capacitor linked to a voltage integrator indicated the stored charge. Using the following relationship

$$q = CV \tag{28}$$

where q is the charge per electron, C is the capacitance, and V is the accumulated voltage as indicated by the integrator, the number of electrons can be solved for as

$$N = CV/q \tag{29}$$

where N is the total number of electrons that have passed through the SEM. Previous studies done in characterizing the NPSAL LINAC have shown that the SEM is only 6% efficient in its' electron collection process [Ref. 18]. Therefore, the total number of electrons can be expressed as

$$N = CV/0.06q \qquad (30)$$

It is the usual custom to discuss irradiation studies in terms of beam fluence which is the number of particles per unit area. Therefore

$$\text{FLUENCE} = \phi = \text{N/BEAM AREA} = CV/0.06qA \qquad (31)$$

where A is the area of the electron beam. This is the form used throughout this study for calculation of beam fluences.

Figure 7 depicts the general layout of the NPSAL LINAC area. A more detailed description of the LINAC and its capabilities can be found in Reference 18.

1. Device Irradiation Procedures

After characterization, the devices where mounted on an aluminum target ladder. The ladder was then placed inside the target chamber. The chamber was evacuated to 10^{-6} Torr and runs were done at ambient temperature. Figure 8 shows a representation of the set-up within the target

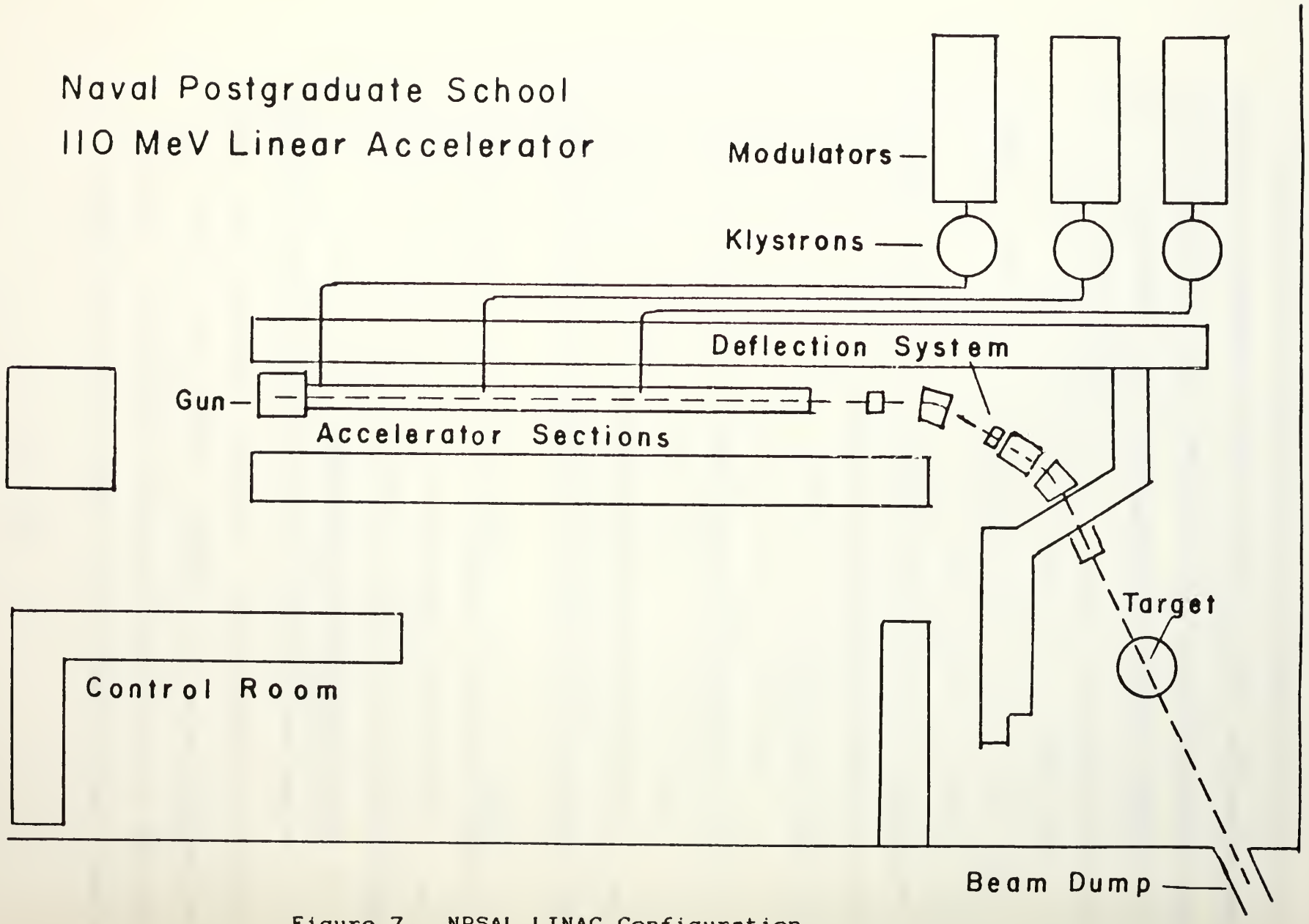

Figure 7. NPSAL LINAC Configuration

chamber. During irradiation, the devices had constant voltage supplied to them by a power supply located external to the target chamber. A series resistor was not used. This was done in an effort to better simulate real-life conditions.

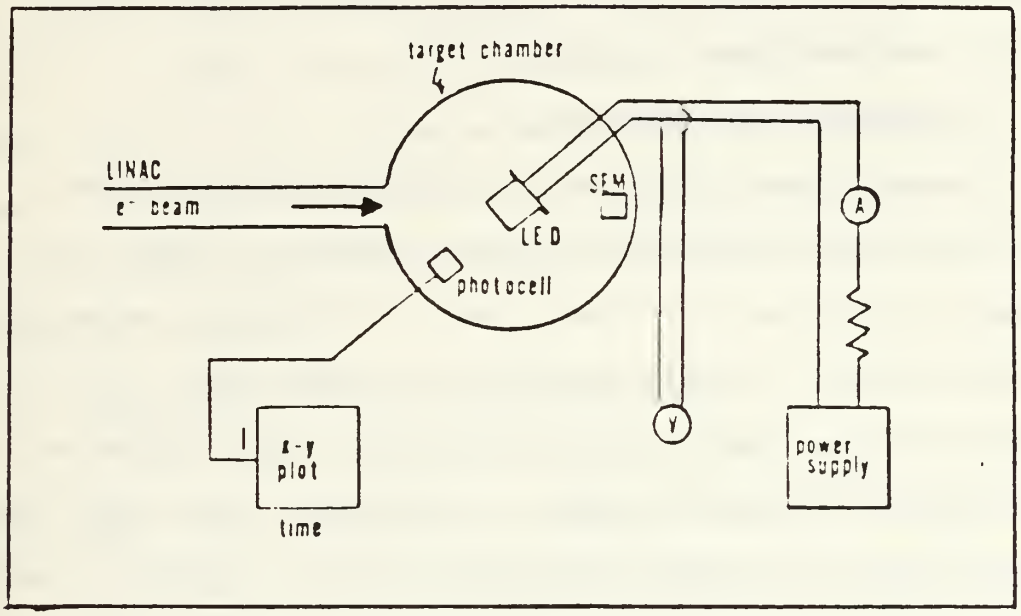

Figure 8. Experimental Configuration in Target Chamber [Ref. 19, p. 39]

A photodetector was used inside of the chamber to measure the change in light output of the devices during irradiation. This measurement used only relative values of light intensity since the photodetector was not calibrated for the characteristic wavelength of the device. The photodetector was attached to an X-Y plotter to provide relative intensity versus duration of irradiation plot. The

abscissa was converted from time to accumulated fluence by dividing the total fluence by the total time of irradiation thereby arriving a scaling factor in units of electrons/cm^2-sec or beam flux. Each device was irradiated until the relative light output was reduced to less than 50% of the initial light output. Experimental results are contained in Chapter IV.

2. Radiation Loss Studies

As mentioned previously, a 30 MeV electron beam should lie within the region where radiative losses are dominant if Gallium or Arsenic are the absorbing materials. In consideration of this, eight additional LEDs, all from group A5, where characterized in exactly the same manner as described earlier. The "cans" or protective enclosures were removed from four of the devices to allow unimpeded access to the semiconductor chip at the base of the device. The devices were then separated into two equal groups consisting of four diodes each; two with can-on and two with can-off. The irradiation runs were conducted in the following manner: one group of four were irradiated with a zero degree offset to the beam axis (beam is perpendicular to the base of the device), the other group was irradiated at a forty-five degree offset to the beam axis (beam axis and device base form a 45^o angle). In this manner, it was hoped to show a significant reduction in the total fluence required for a specified degradation in output light intensity between the

can-on and can-off groups. It was theorized that the group of devices that had their can-on should require less fluence to cause the same amount of degradation. This was expected due to the effect of the Bremsstrahlung process creating a shower of electrons as the beam traversed the protective can, thereby exposing the semiconductor at the base of the device to a larger number of electrons. The procedure whereby some of the devices were installed at a 45° angle to the beam axis was done to see if increasing the distance that the electrons traversed through the metal enhanced this effect.

3. Beam Cross-Section Characterization

Fluence calculations previous to this work at the NPSAL LINAC, were based on an "optical" area of the electron beam. At the top of the target ladder, there is a phosphor screen marked out with a grid pattern. Prior to irradiation of a device, this screen was placed in the beam to facilitate beam focusing and by observing the size of the beam spot, the area could be calculated. Also, an assumption that the beam exhibited a rectangular pulse-type distribution (i.e. the density of electrons was constant across the entire cross-section) was made. In an effort to better characterize the beam in terms of cross-section and electron distribution, a simple device was constructed of two uninsulated wires arrayed in a cross-hair fashion and attached to a piece of bakelite. These wires, when exposed

to the electron beam , would give a detectable voltage reading which could be used as a signal as "being in the beam". Ideally, this signal would be proportional to the electron fluence in the beam at that location.

First, a determination had to be made if the voltage signal from the wire target would be comparable to signals from commercial test equipment, whose reliability was known. The wire target was connected to a voltage integrator through the SEM and exposed to the beam for a period of time. By equation (28) and

$$I = q/t \tag{32}$$

the accumulated voltage reading was converted to a current reading. This was compared to the known beam current as measured by the Beckman Multimeter located in the LINAC control room. Figure 9 shows that a linear relationship exists between the Beckman current and both the vertical and horizontal wire axis current readings. Thus, it was felt that the data obtained from the wire target would indeed be proportional to the beam intensity.

The next step was to use the wire target to determine the profile of the beam in both the horizontal and vertical axes. Note: interpretation of vertical and horizontal axis in this context should be as follows. The wire target lies in the X-Y plane with the beam axis along the Z coordinate.

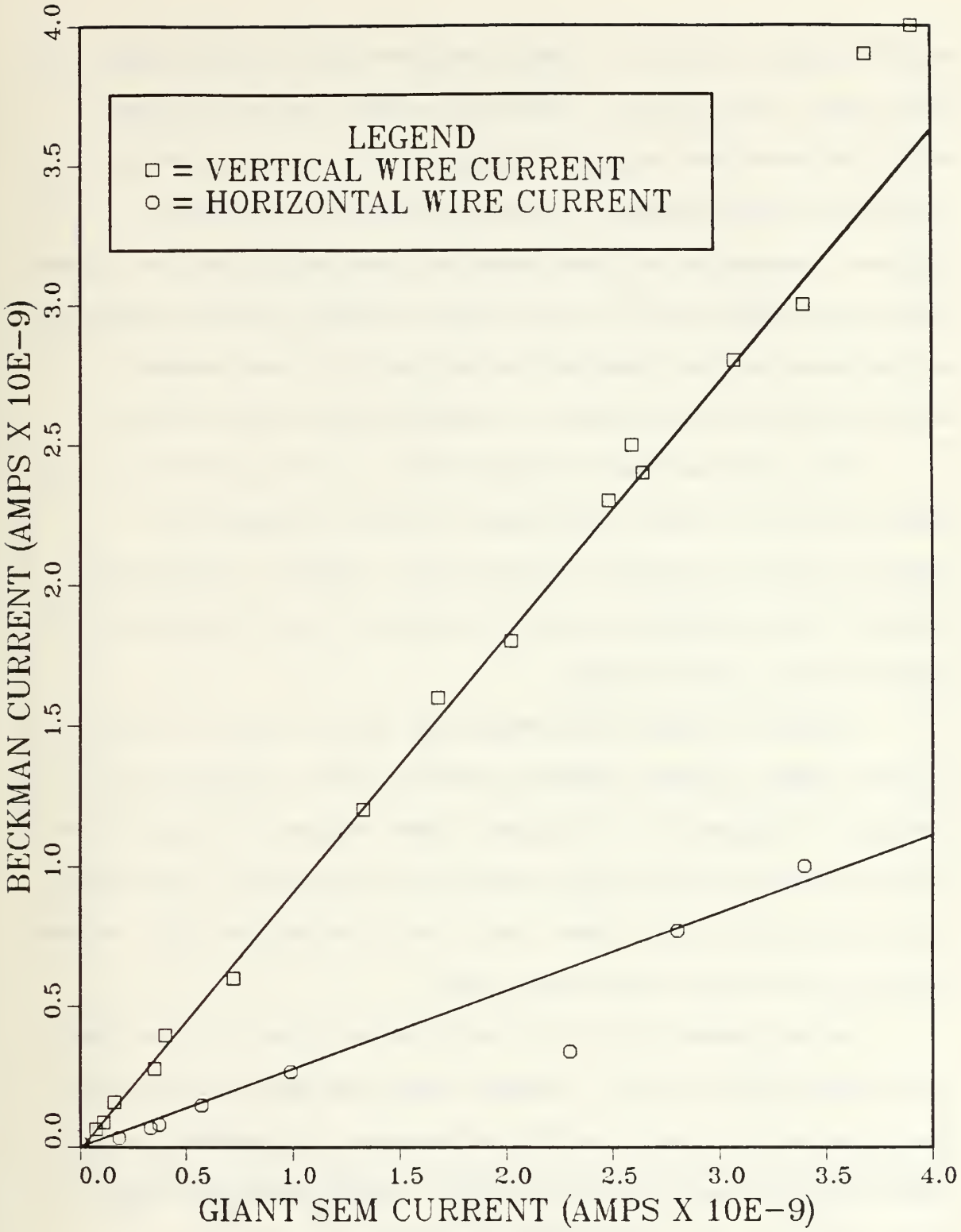

Figure 9. Beckman (wire target) Current versus SEM Current for Both Horizontal and Vertical Wires

The horizontal axis = X; the vertical axis = Y. For the horizontal axis profile, the wire target was held steady while the beam was steered through the vertical wire by controlling the magnets located in the final section. Angular increments of beam steering were converted to linear distances across the wire by taking visual position reading of the beam on the phosphor screen for the same magnet settings. At each setting, a voltage reading was taken.

For the vertical axis profile, the beam was held steady while the wire was moved through the beam by a stepping motor attached to the target ladder. The voltage results were recorded on an X-Y plotter with X being the distance and Y the voltage.

After the data was normalized using Figure 9, the apparent beam current density versus linear distance was plotted in Figure 10. It appears that the beam resembles an ellipse with its major axis along the horizontal direction. This elliptical area, then, was used in equation (31) versus the previously used "optical" area.

As an example of the significance that this revised area determination has, consider that the beam used for the characterization was visually determined to resemble a rectangle with an area of 1.51 cm^2. After profiling the beam with the wire target, the elliptical area was determined to be 0.52 cm^2, which is a 1/3 reduction in beam area estimation. Since fluence is inversely

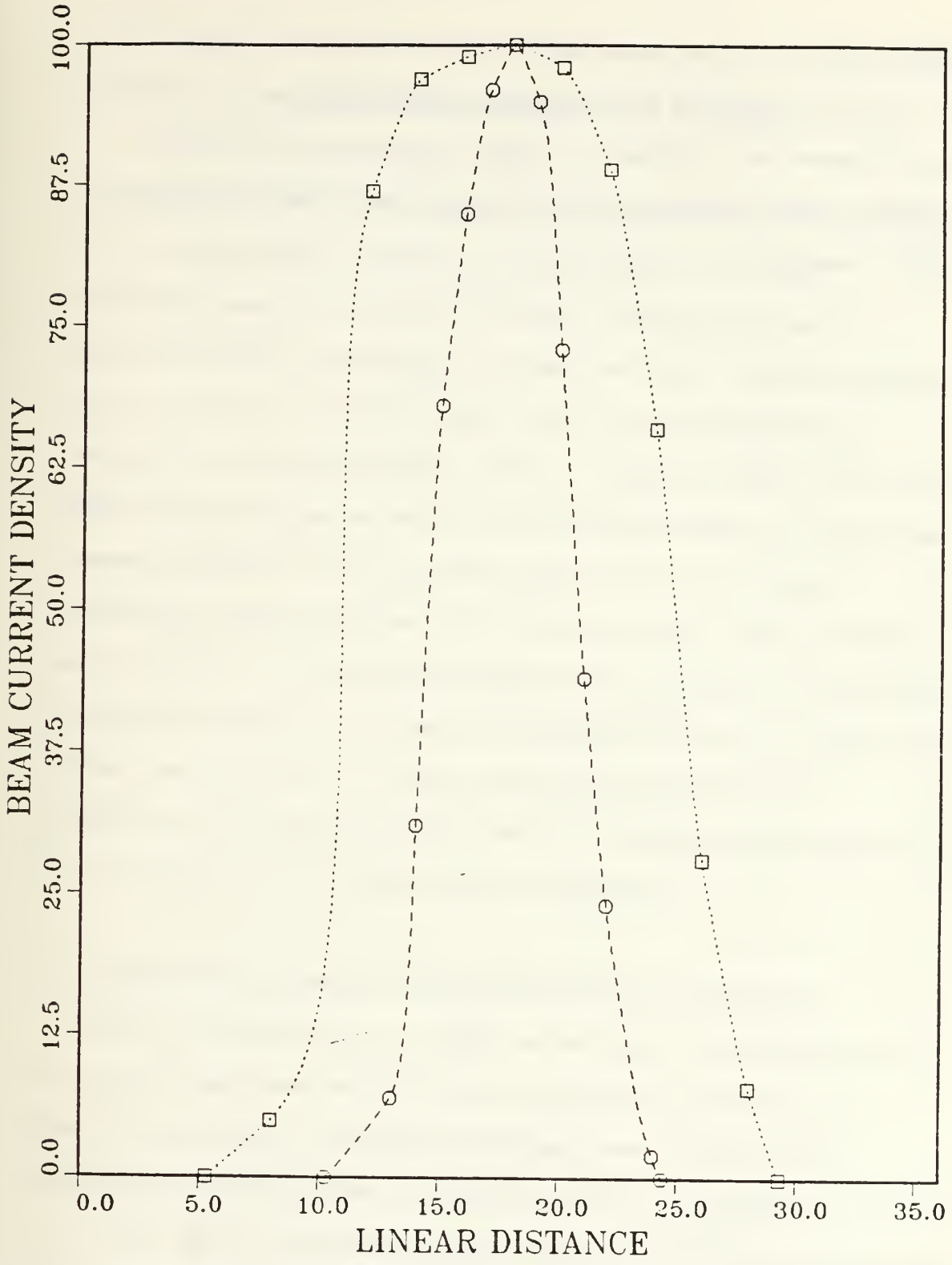

Figure 10. Apparent Beam Current Density versus Linear Distance as Determined From Wire Target Experiment.(Square plot symbols indicate horizontal axis, round symbols indicate vertical axis.)

proportional to the cross-sectional area of the electron beam, this reduction in beam area results in an increase of beam fluence by a factor of three. Appendix A contains expanded calculations concerning the relevance of the beam profile work.

IV. EXPERIMENTAL RESULTS AND ANALYSIS

This chapter will present the experimental results found from irradiation of $GaAs_{.7}P_{.3}$ LEDs with a 30 MeV electron beam. The effects of this irradiation on the characteristic wavelength, current-voltage relationships, and the light intensity output will be discussed and presented both graphically and in tabular form. The current controlling mechanism will be determined and the lifetime damage constant will be calculated for all groups. A graphical interpretation of relative light output versus beam fluence is included. Comparison of fluence requirements between the can-on and can-off groups for both a zero degree offset and 45° tilt to the beam axis is presented. Conclusions concerning the present work and some suggestions for future work are contained in Chapter V.

A. IRRADIATION EFFECTS ON CHARACTERISTIC WAVELENGTH

After irradiation, the LEDs were again characterized as to their peak wavelength using a modified Beckman DK-1A Spectrophotometer. Results of these post-irradiation measurements indicated a characteristic wavelength of 718nm vice the 720nm wavelength found before irradiation. However, due to the 5nm resolution of the Beckman, these results were

felt to indicate that no significant alteration of the characteristic wavelength had occurred.

B. IRRADIATION EFFECT ON CURRENT-VOLTAGE CHARACTERISTICS

1. Current-Voltage Data

Figures 11 through 16 depict the current versus forward bias voltage characteristics for both pre and post irradiation conditions. The data was obtained as described in Chapter III at a constant temperature of 30°C. Associated with each of the three groups are two graphs. One graph depicts the full scale amperage starting from the initially detectable signal of 1 microamp to the upper limit of current used, 100 milliamps. The second graph shows an expanded current scale from 1 to 100 milliamps were the bulk of the data was taken. Note that in all the graphs in this section, the solid line indicate a pre-irradiation condition while the dotted line is for data taken after irradiation. The numbers quoted in the legends are the number designations for the LEDs used for cataloging the devices within each group.

Preliminary observations of these graphs indicate that current for a given forward bias voltage increased after irradiation in all the groups with the exception of LED #486 in group A5. It is observed to have less current for a given forward bias voltage when the voltage exceeds approximately 1.540 volts. The average current gains for a

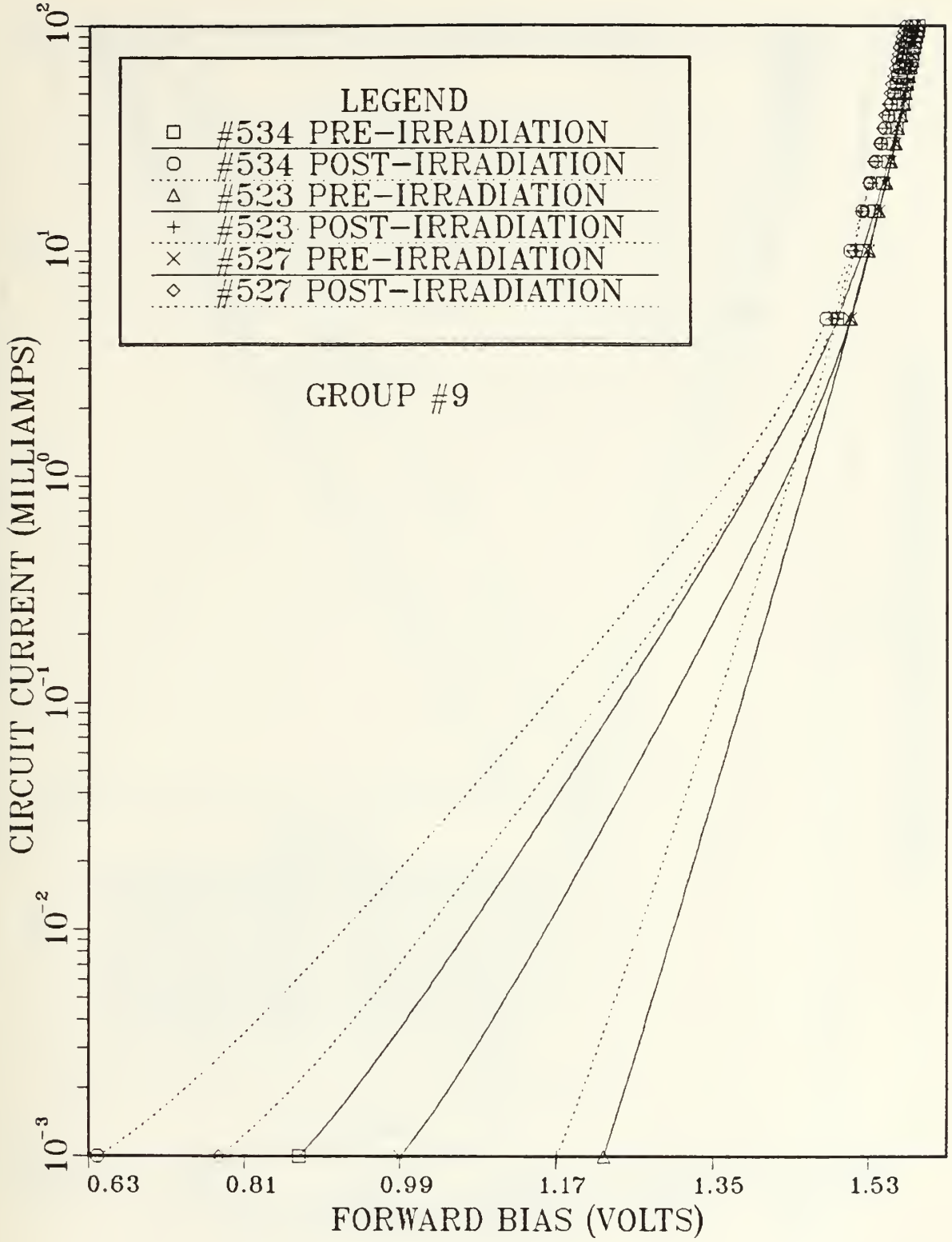

Figure 11. I-V Characteristics for 3 LEDs in Group 9
(— before irradiation, ... after)

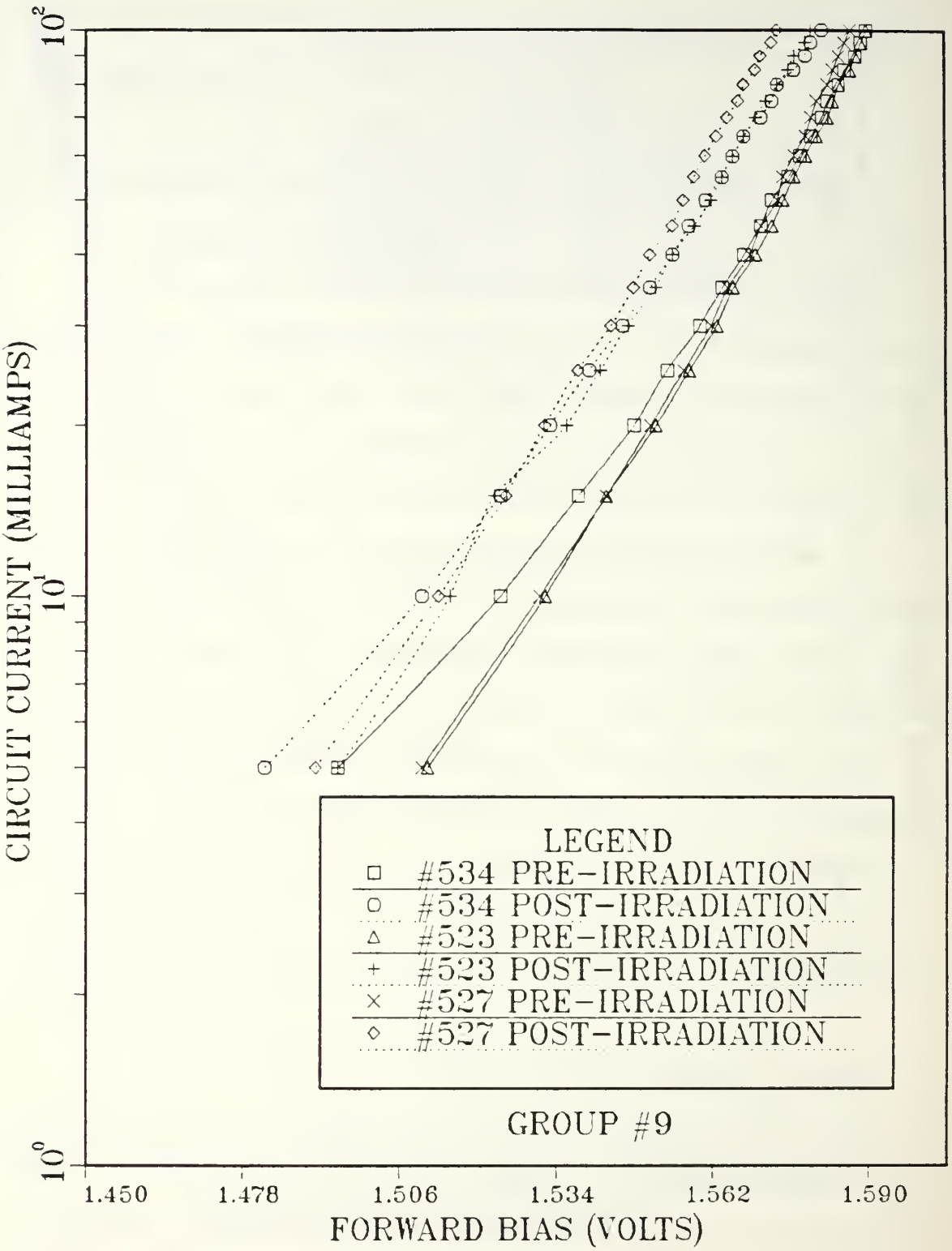

Figure 12. I-V Characteristics for 3 LEDs in Group 9 (expanded scale)

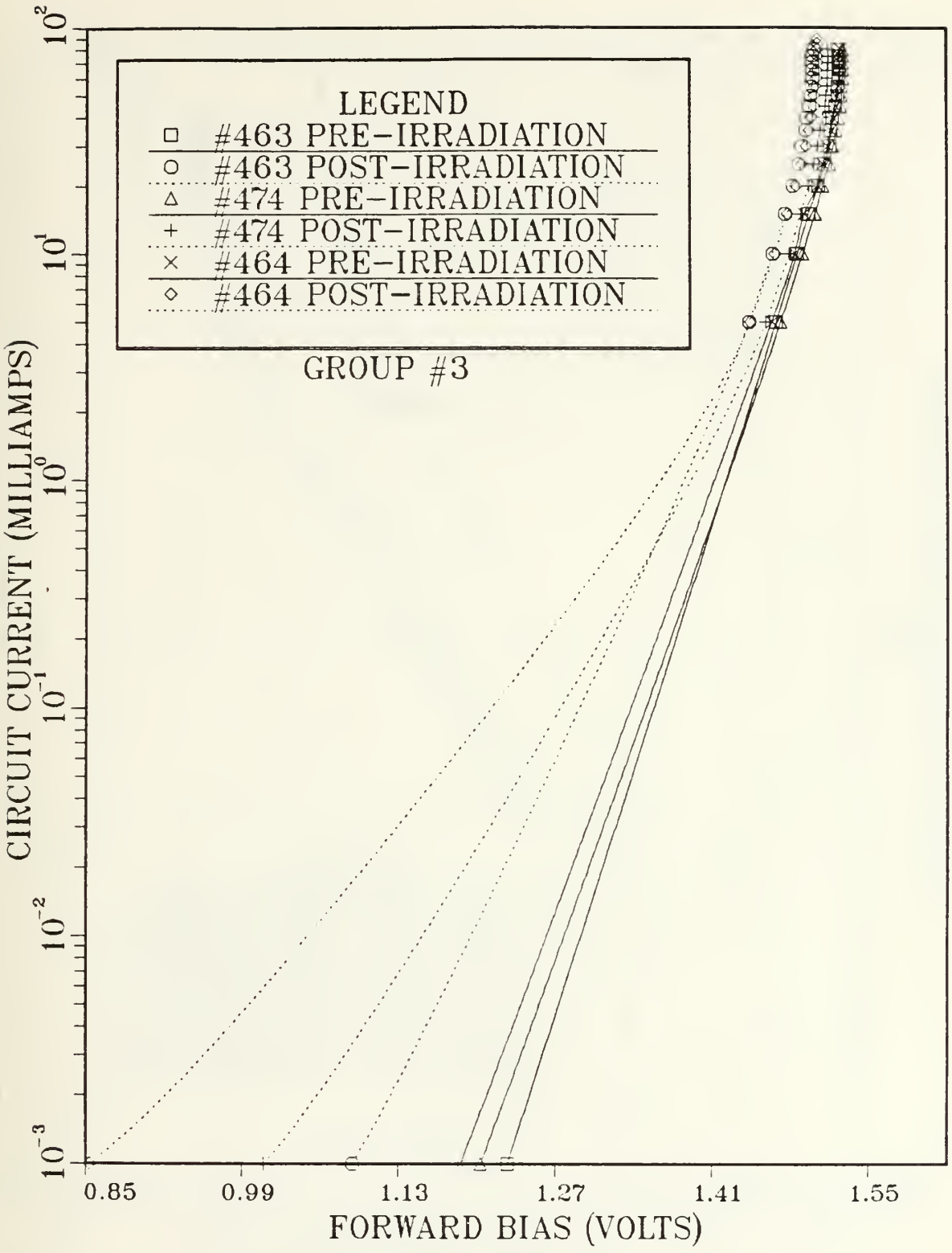

Figure 13. I-V Characteristics for 3 LEDs in Group 3
(— before irradiation, ... after)

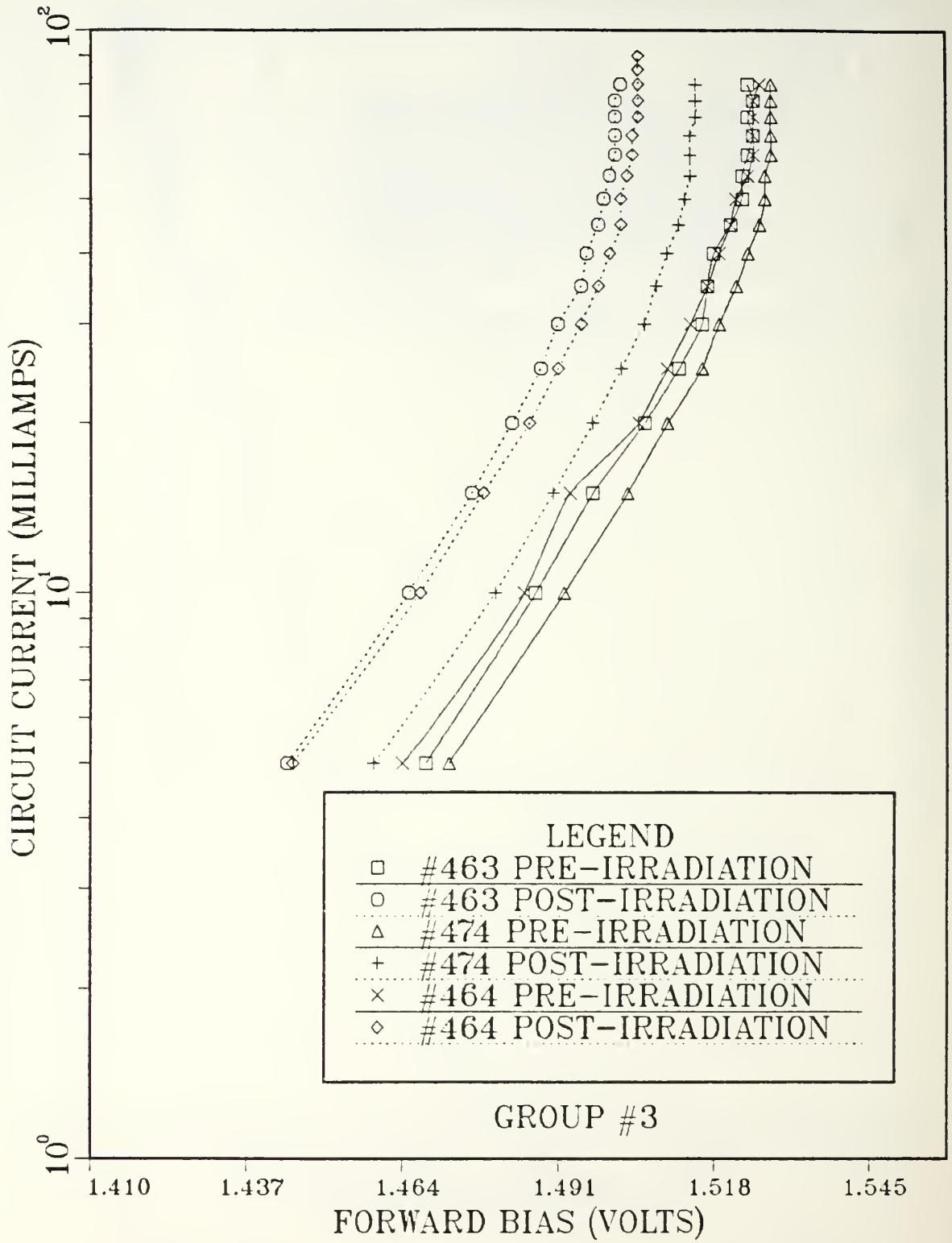

Figure 14. I-V Characteristics for 3 LEDs in Group 3 (expanded scale)

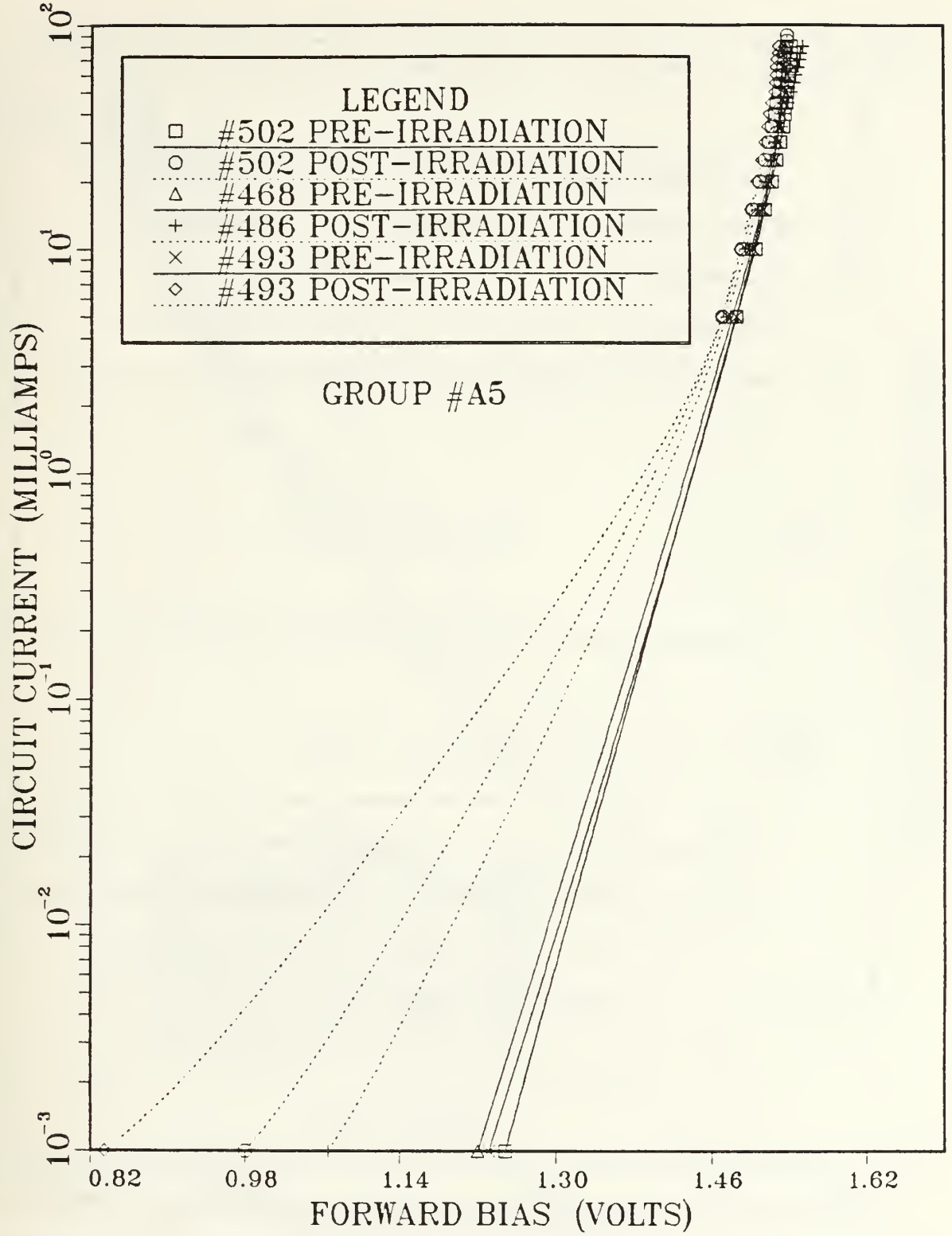

Figure 15. I-V Characteristics for 3 LEDs in Group A5
(— before irradiation, ... after)

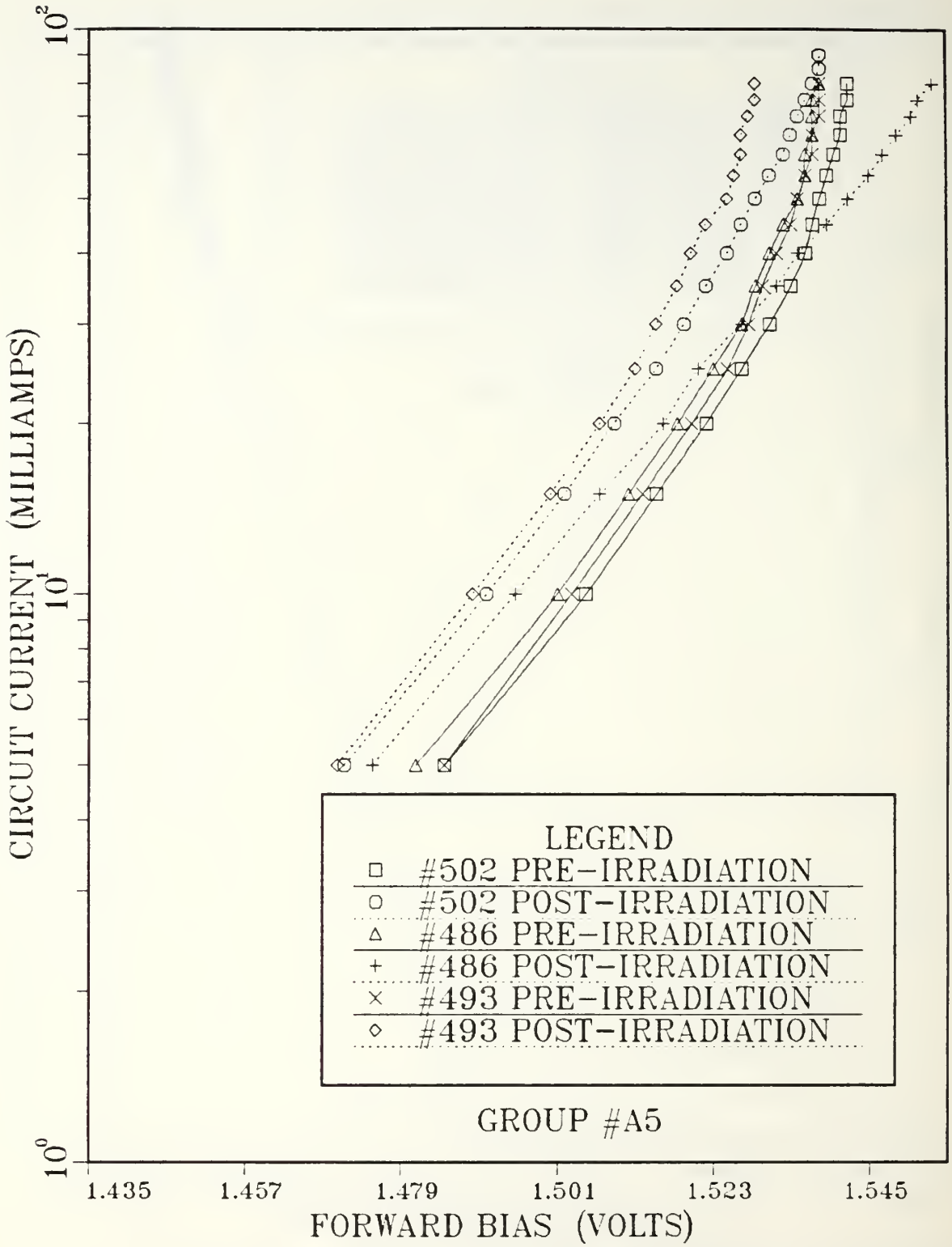

Figure 16. I-V Characteristics for 3 LEDs in Group A5 (expanded scale)

given voltage are 1% for both group 9 and A5, and 1.2% for group 3.

2. Current Controlling Mechanism Determination

In Chapter II, a description of the two types of current controlling mechanisms were given. Equation (12) gave a relationship that could be used to determine if diffusion or space-charge recombination current was the dominant process.

$$I_F \approx \exp(qV_a/nkT) \qquad (12)$$

Taking the natural logarithm of both sides yields

$$\ln(I_F) = qV_a/nkT \qquad (33)$$

If $\ln(I_F)$ is plotted versus V_a, a straight line of slope q/nkT should result. Thus, on a semilog plot

$$n = (q/kT)2.3(\text{slope}) \qquad (34)$$

If n = 1 diffusion controlled current dominates and if n = 2, space-charge recombination current dominates. The slope calculations were done using the "straight-line' portions of the curves contained in Figures 11 through 16 and two values of n were calculated: n_o which represents

pre-irradiation values, and nI which represents post-irradiation values. These calculated values of n are included in Table I. They show that all the devices tested were diffusion controlled, both before and after irradiation.

C. IRRADIATION EFFECTS ON ABSOLUTE LIGHT OUTPUT INTENSITY

Figures 17 through 19 show the absolute light output intensity, as measured by the 550 fiber optic power meter, versus forward current. Again, each plot contains a single group with the solid lines indicating pre-irradiation values and dotted line for values taken after irradiation. Observations indicated that the output intensity for a given current decreased after irradiation. This is consistent with the theories that the irradiation produces non-radiative recombination centers within the lattice which compete for the injected carriers. This results in an overall loss of light output intensity. On the average, group 9 suffered a 55% reduction in light output intensity, group A5 a 45% loss, and group 3 loosing 65% of its initial intensity. However, it should be pointed out that in terms of received dose, group 3 averaged the highest (1.46×10^{14} e/cm^2), then group 9 (8.06×10^{13} e/cm^2), and A5 received the least dose, (2.97×10^{13} e/cm^2).

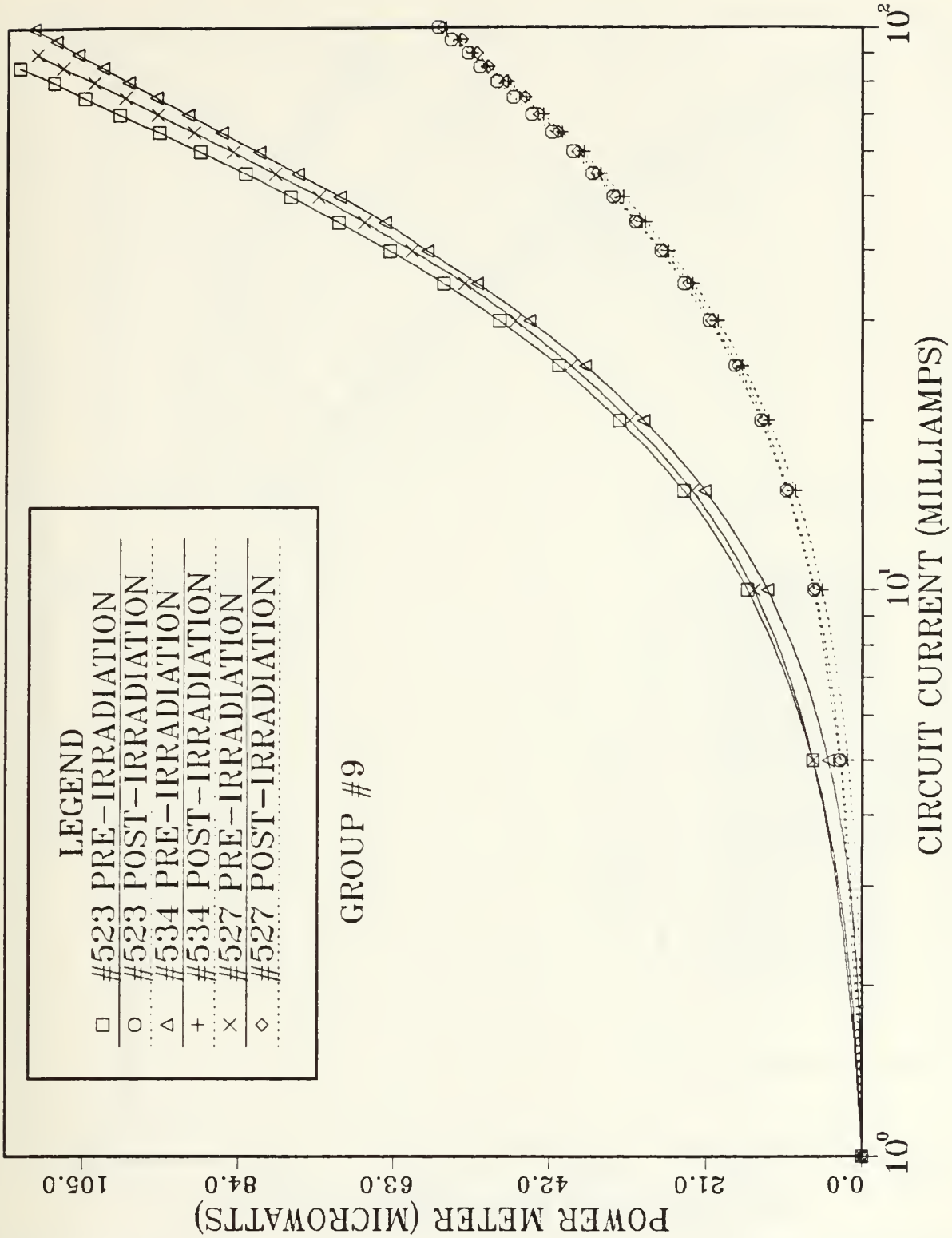

Figure 17. Absolute Light Output versus Current for 3 LEDs in Group 9 (— before irradiation, ... after)

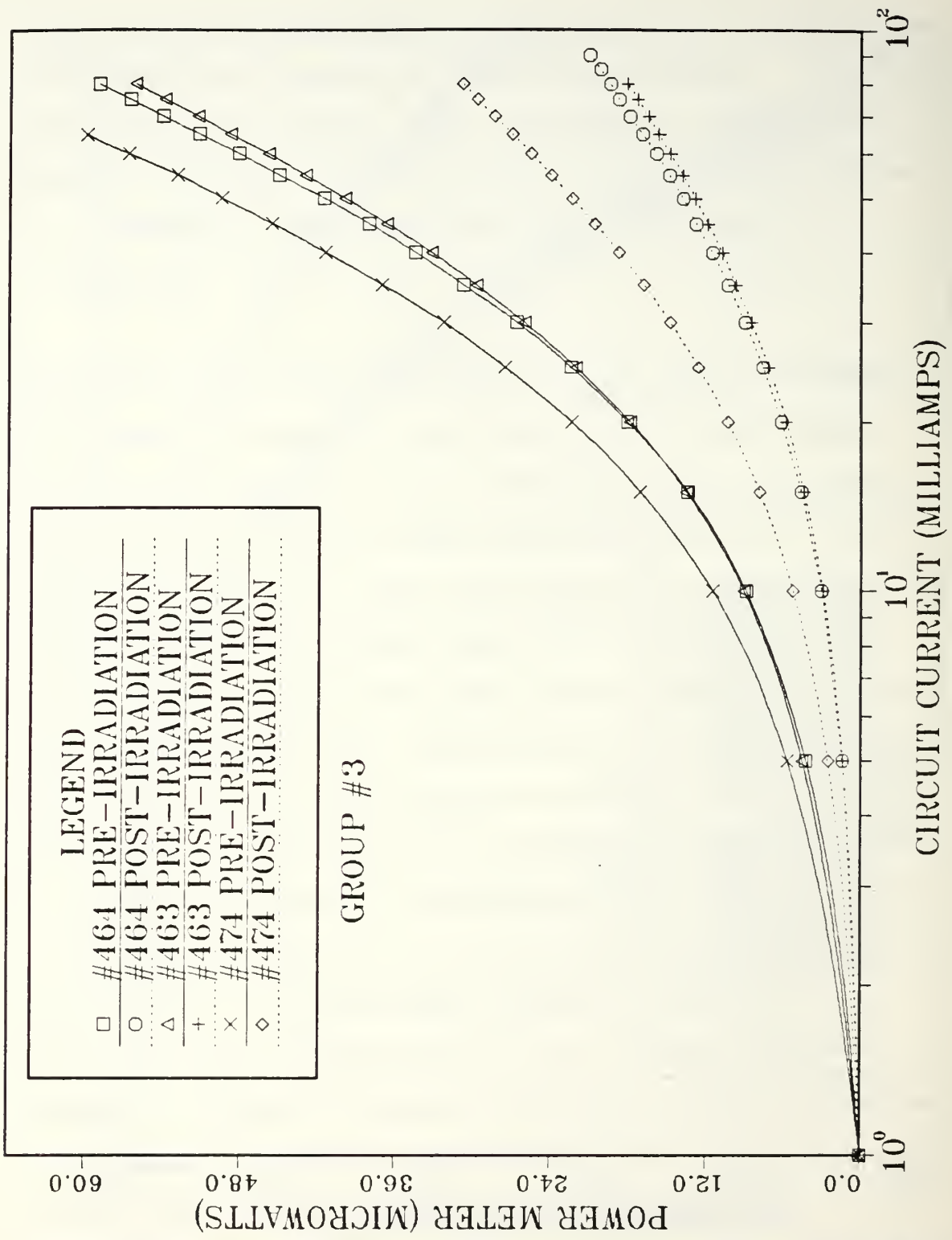

Figure 18. Absolute Light Output versus Current for 3 LEDs in Group 3 (— before irradiation, ... after)

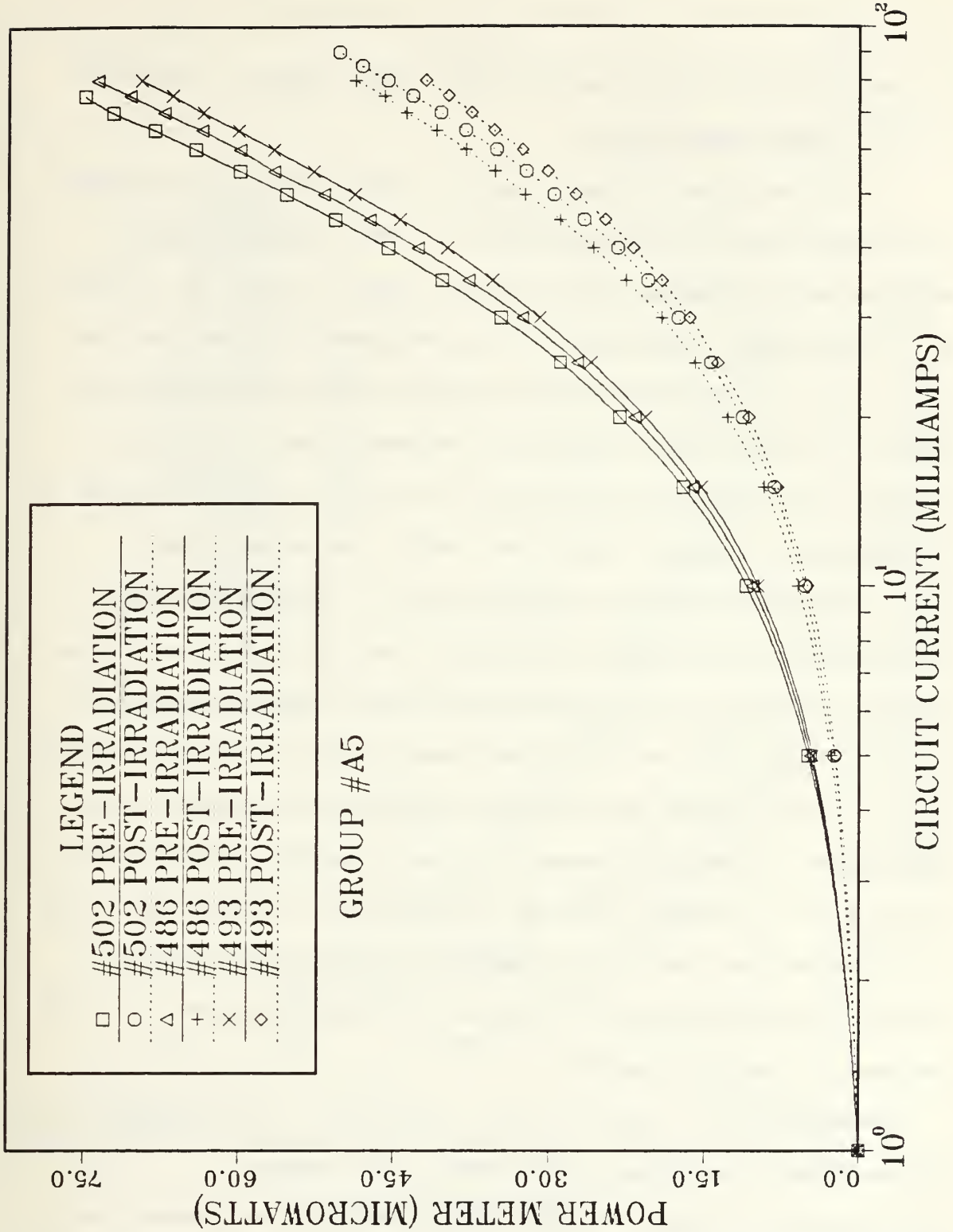

Figure 19. Absolute Light Output versus Current for 3 LEDs in Group A5 (— before irradiation, ... after)

D. IRRADIATION EFFECTS ON RELATIVE LIGHT OUTPUT INTENSITY

1. Light Output Data

In addition to the absolute light output measurement discussed above, a photodetector in the target chamber enabled us to examine the relative light output of the LED as it underwent irradiation. The photodetector output was fed to an X-Y recorder which produced a real-time plot of relative light output intensity versus time. Figures 20 through 22 shows this information with the X axis altered to indicate the fluence (electron /cm^2) instead of time. This transformation was accomplished by taking the total accumulated fluence and dividing it by the run time. These derived units of flux (electron/cm^2-sec) where then used to transpose each unit of time into a unit of fluence. Note that in the legend, the number quoted in the parenthesis indicated the total fluence that each device was exposed to. The Y axis in these plots is the intensity of the device at any time during the run divided by the maximum intensity shown at the beginning of the run. This then gives units of percent of initial output.

Although not a topic of this research, the annealing properties of $GaAs_{1-x}P_x$ LEDs are a well known phenomenon. Evidence of some annealing at room temperature can be observed in Figure 21 for devices #463 and #464. During irradiation of the device, the run time of the procedure occasionally exceeded the time scale of the X-Y

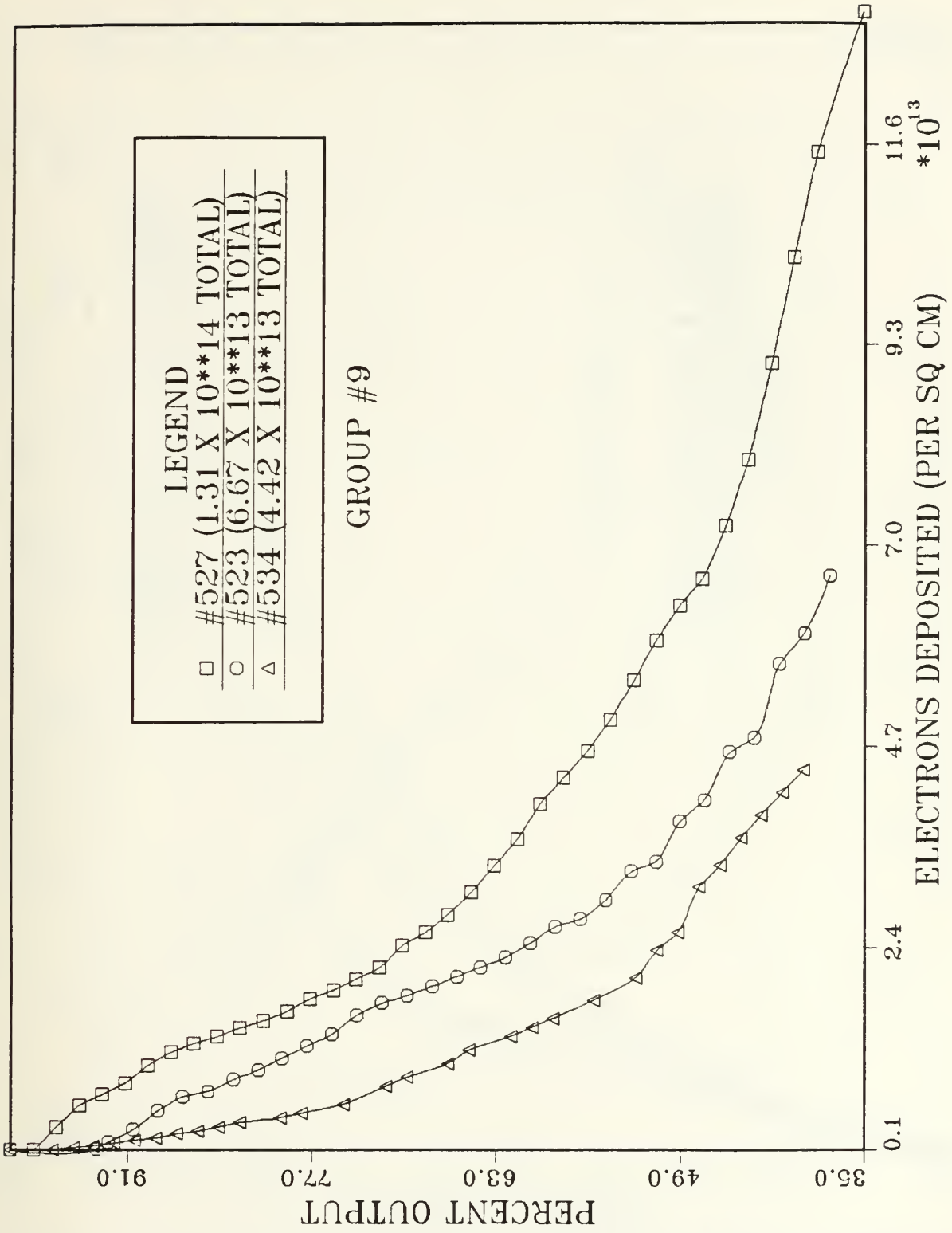

Figure 20. Relative Light Output versus Accumulated Electron Dose for 3 LEDs in Group 9

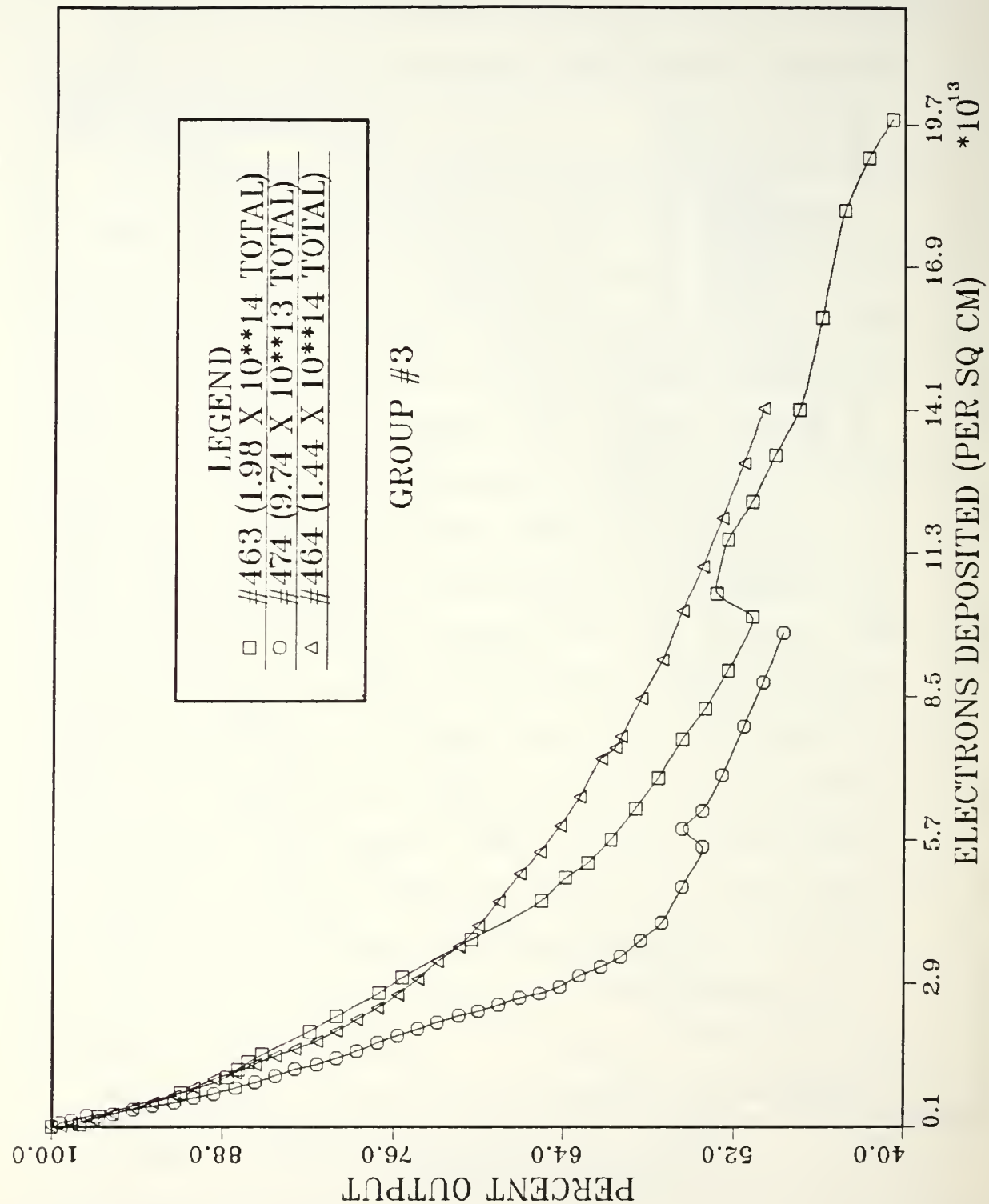

Figure 21. Relative Light Output versus Accumulated Electron Dose for 3 LEDs in Group 3

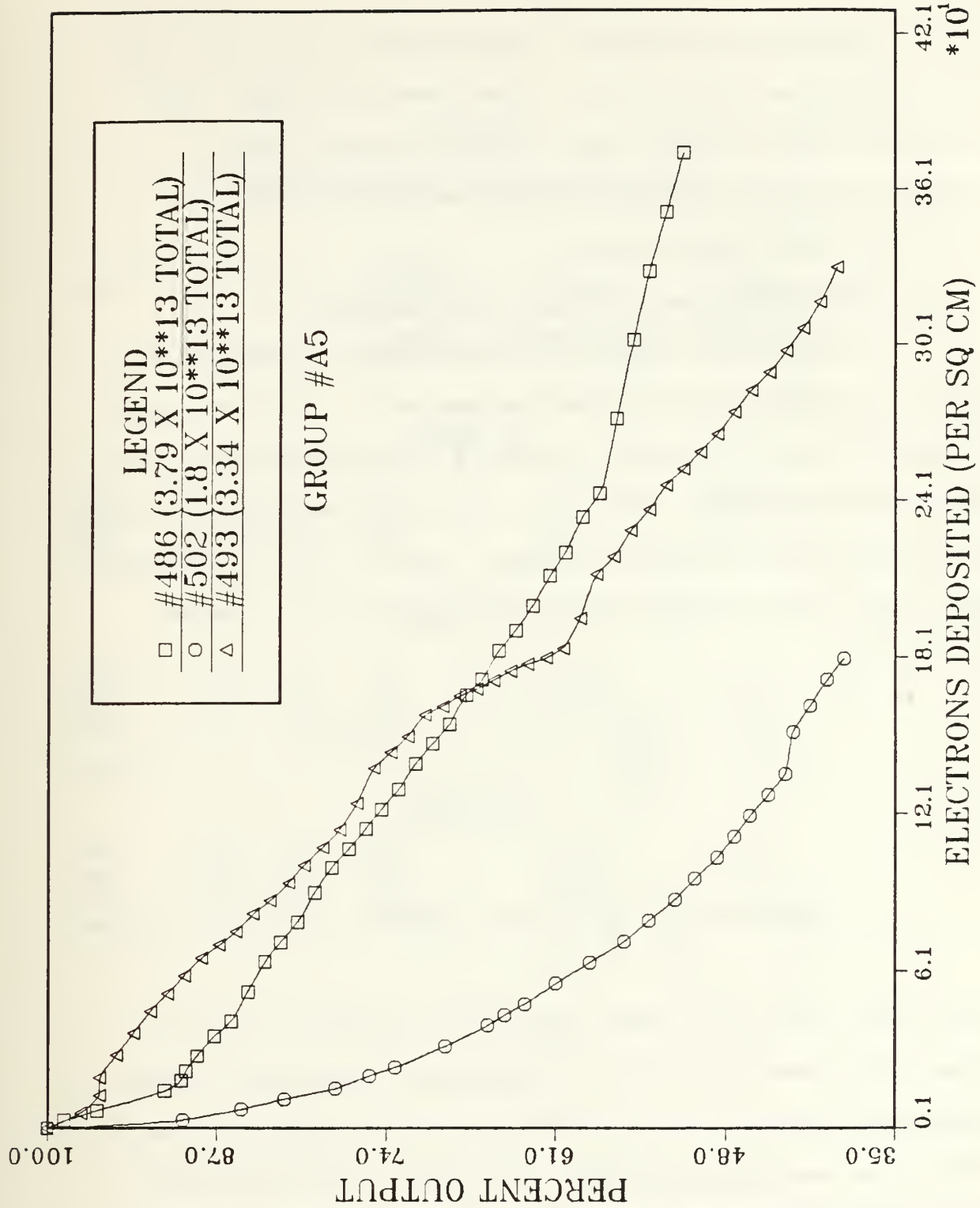

Figure 22. Relative Light Output versus Accumulated Electron Dose for 3 LEDs in Group A5

plotter. When this occurred, the beam was shut down while the plotter was reset with a clean sheet of paper. This procedure rarely took longer than 10 seconds yet an annealing of approximately 2% can be observed in the relative light output curves.

2. Lifetime Damage Constant Calculations

As derived in Chapter II, Equations 11 through 16 outline a mathematical procedure whereby a lifetime damage constant can be calculated. Knowing that the devices are diffusion controlled (Table I), and that they were run under the condition of constant voltage, Equation (26), reproduced here, will be the basis for the calculation for damage constants

$$\frac{\tau_0}{\tau} = \frac{L_0}{L} = 1 + \tau_0 K \phi \qquad (26)$$

or

$$\left(\frac{L_0}{L} - 1\right)\left(\phi\right)^{-1} = \tau_0 K \qquad (35)$$

The values for (L_0/L) were taken from Figures 20 through 22 at point where the lines maintained a relatively steady slope and prior to any inflection points. Tabular values of the damage constant are given in Table I. Note that the Y axis for Figures 20 through 22 are L/L_0. Therefore, it was necessary to convert these values back into decimal form

TABLE I

CHARACTERISTIC VALUES FOR LEDs

LED #	n_o	n_I	TOTAL FLUENCE (10^{13}) (e/cm^2)	FLUX (10^{12}) (e/cm^2-sec)	T_oK (10^{-14}) (cm^2/e)
			GROUP 9		
534	1.3	1.3	4.4	1.0	4.4
523	1.1	1.1	6.7	1.1	2.7
527	1.0	1.1	13.	1.0	1.7
			GROUP 3		
463	0.9	0.9	20.	1.5	1.1
474	0.9	0.9	9.7	0.87	1.9
464	0.9	0.9	14.	1.1	1.1
			GROUP A5		
486	0.9	1.1	3.8	.76	3.0
493	0.8	0.9	3.3	.68	3.6
502	0.9	1.0	1.8	.80	1.1

(i.e. 45% = 0.45) and invert this value to arrive at the desired value of L_o/L.

E. RADIATIVE LOSS RESULTS

A comparison of results between devices irradiated in a can-on or can-off configuration is presented in this section. Figures 23 through 26 show the current versus forward bias voltage characteristics for both pre and post irradiated devices. Figures 23 and 24 depict the condition of 0° offset to the beam and Figures 25 and 26 show the 45° offset case. In all plots within this section, the graphical line patterns will have following meanings: solid lines indicate pre-radiation can-on devices, broken solid lines are for the pre-radiation can-off devices, dashed lines are used for post-radiation can-on devices and dotted lines indicate the post-radiation can-off devices.

Preliminary observations indicate that the 0° offset group experienced an approximate increase of current for a given value of voltage after irradiation of 1% while the 45° offset group showed a 1.5% gain. Again, the "straight-line" portions of the curves contained in Figures 23 through 26 were used to determine the slope. This slope was used in Equation (34) to calculate n, which describes the dominant current controlling mechanism. Values for n are contained in Table II.

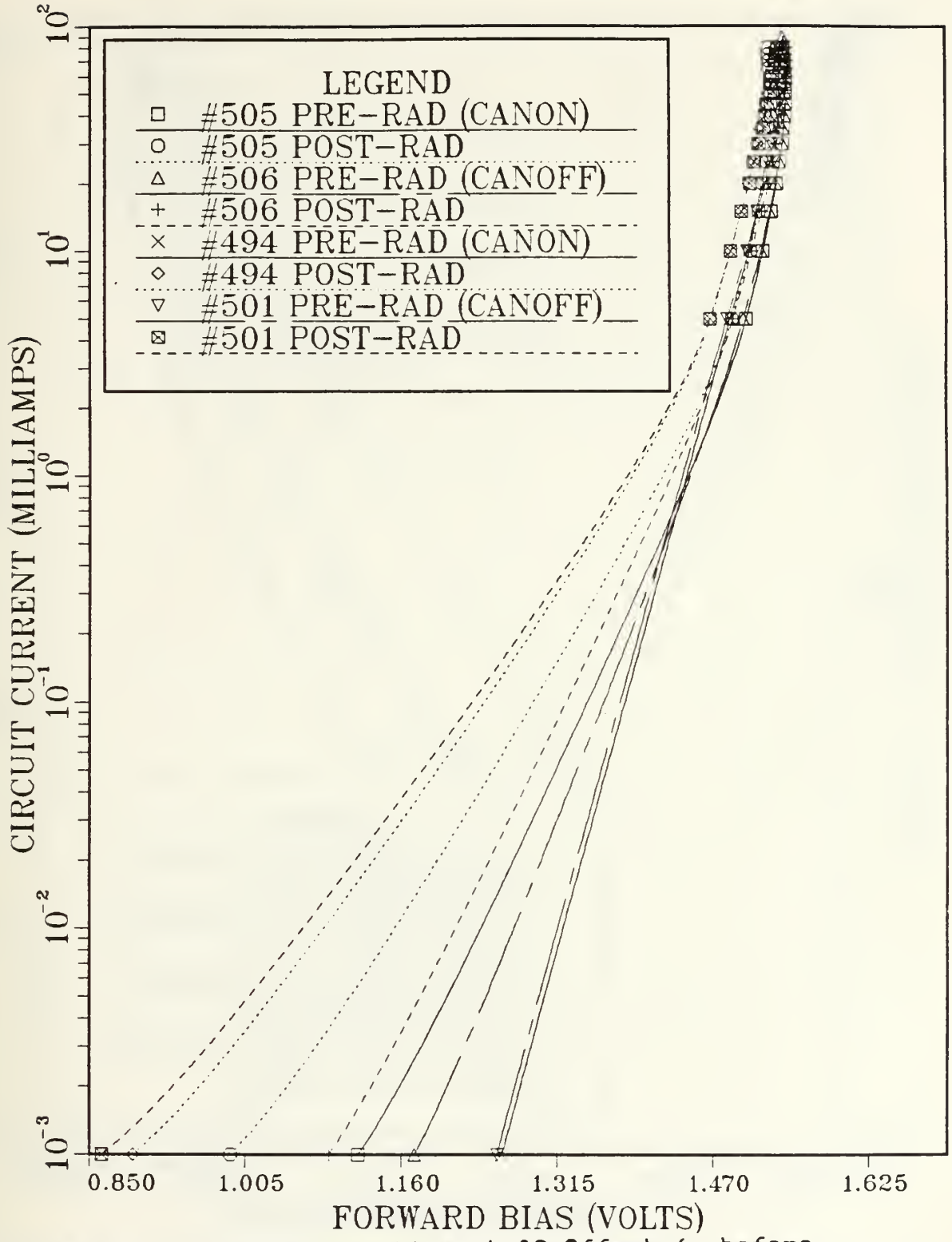

Figure 23. I-V Characteristics at 0° Offset (— before irradiation can-on, ... after can-on, —-— before can-off, --- after can-off)

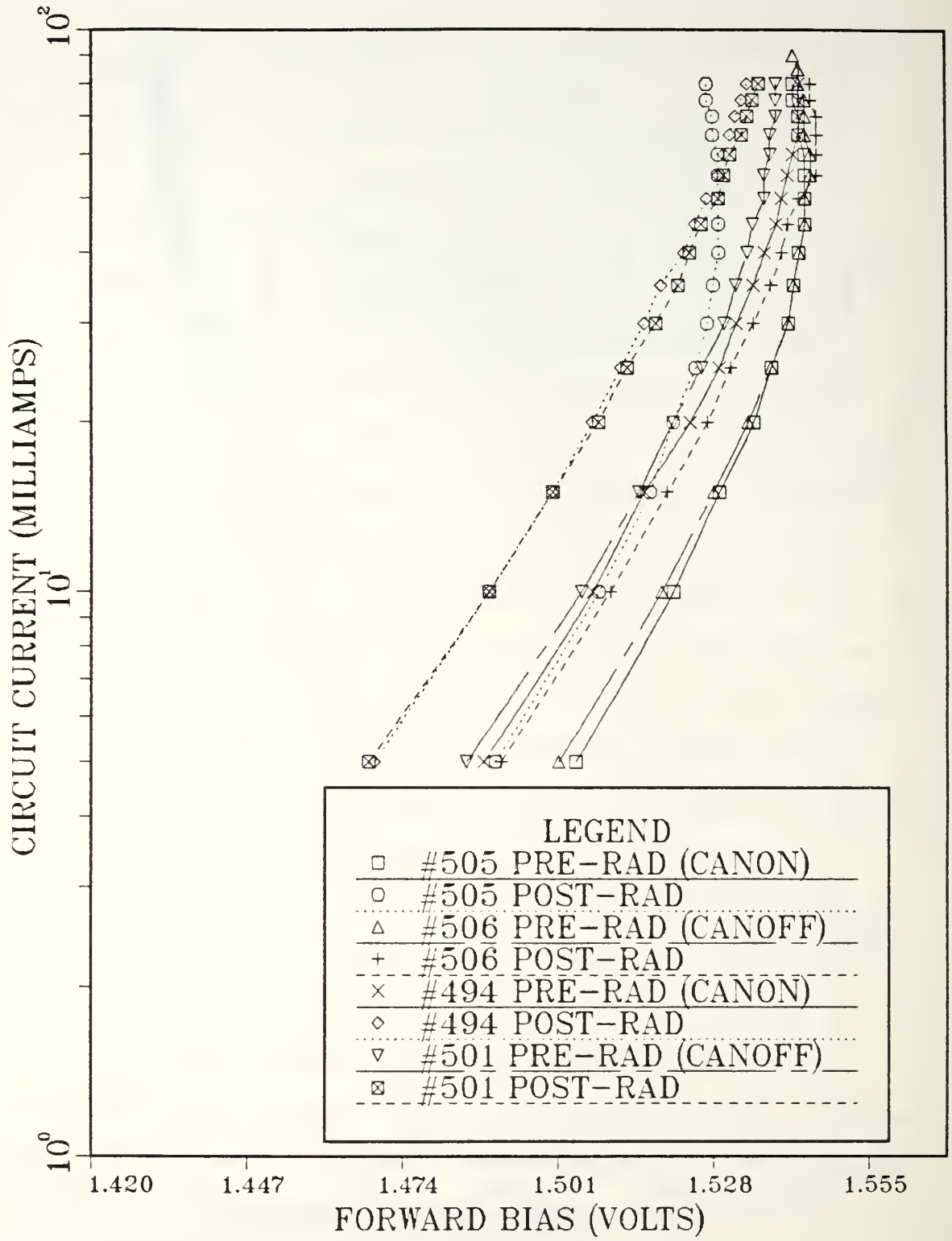

Figure 24. I-V Characteristics at 0° Offset (expanded scale)

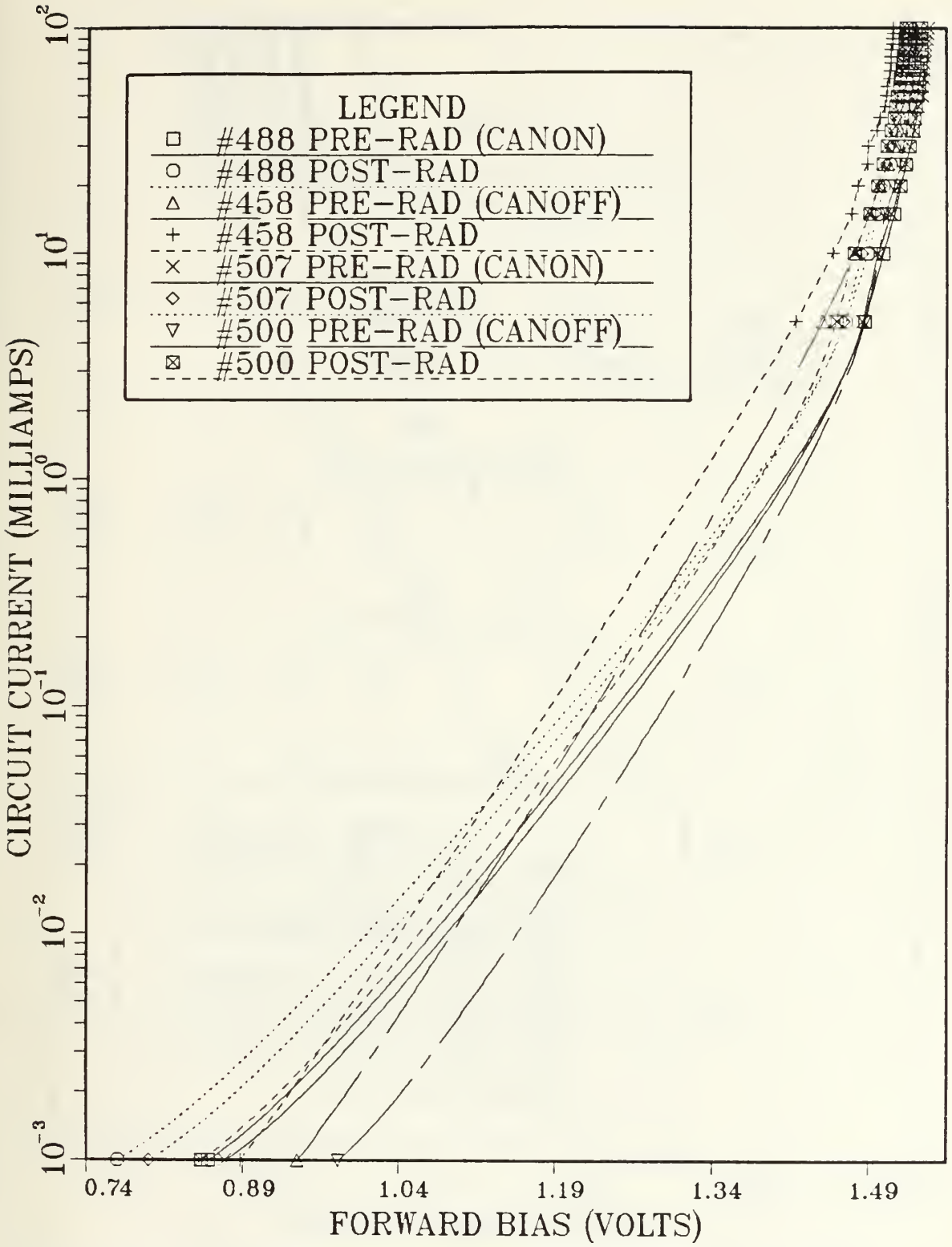

Figure 25. I-V Characteristics at 45° Offset (— before irradiation can-on, ... after can-on, —-— before can-off, --- after can-off)

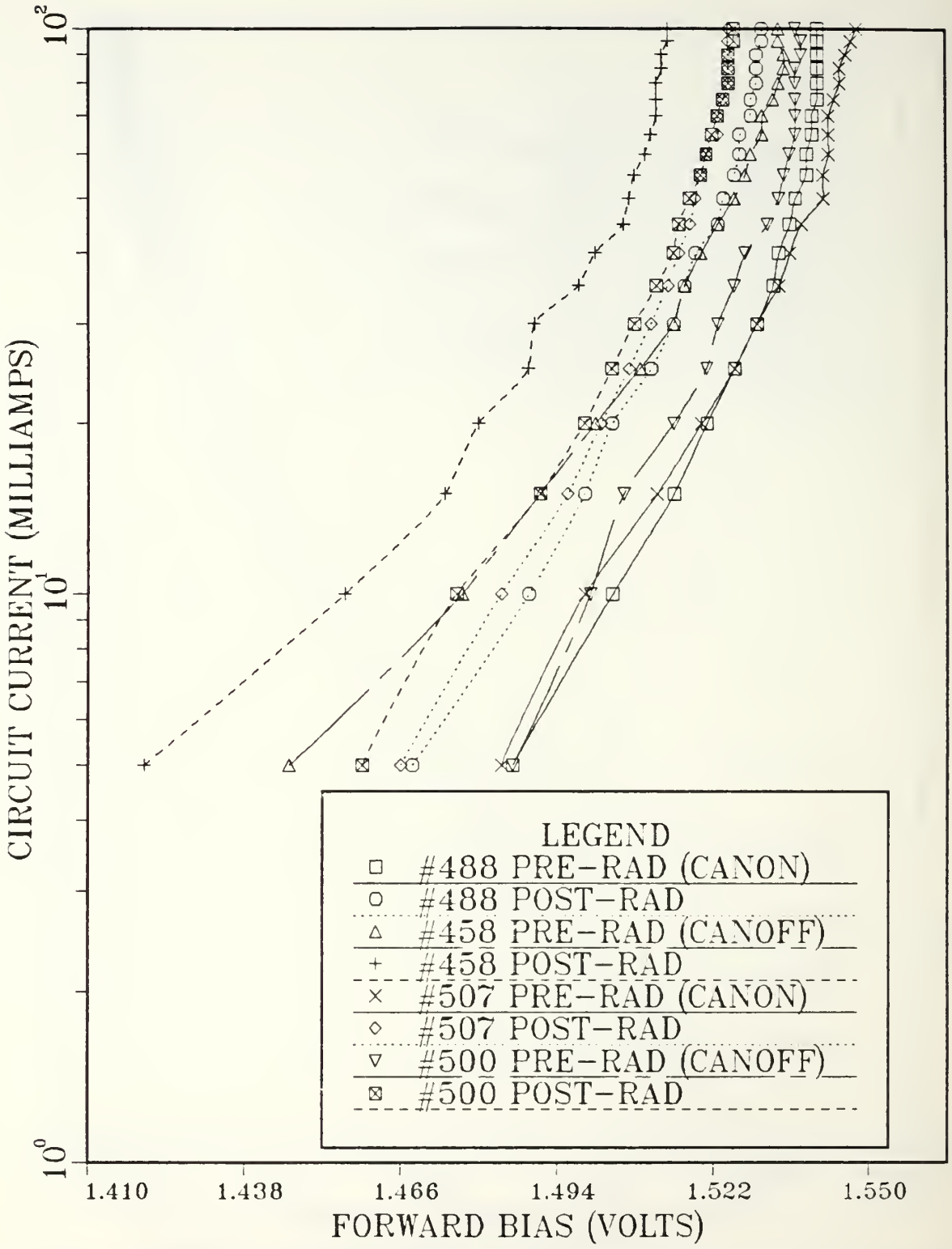

Figure 26. I-V Characteristics at 45° Offset (expanded scale)

TABLE II

CHARACTERISTIC VALUES FOR LEDs
(RADIATIVE LOSSES)

LED #	n_o	n_I	TOTAL FLUENCE (10^{13}) (e/cm^2)	FLUX (10^{12}) (e/cm^2-sec)	T_oK (10^{-14}) (cm^2/e)
			0° OFFSET CAN-ON		
505	0.6	0.6	2.4	.83	4.1
494	0.8	0.9	11.	.89	2.4
			0° OFFSET CAN-OFF		
506	0.7	0.9	4.4	1.3	1.8
501	0.8	1.0	88.	.90	2.9
			45° OFFSET CAN-ON		
488	0.8	0.9	4.9	1.2	2.5
507	1.0	0.9	3.2	1.2	8.1
			45° OFFSET CAN-OFF		
458	1.3	1.4	15.	1.2	1.1
500	0.8	1.0	3.1	.73	3.9

Absolute light intensities as given by the 550 power meter are given in Figures 27 and 28. The trend of less output light intensity at a given value of current after irradiation continues with average losses of 48.5% and 49% for the can-on and can-off respectively at 0° offset and 62% and 62.5% reduction for the can-on and can-off respectively at 45° offset.

The relative light intensity versus accumulated fluence is given if Figures 29 and 30. The damage constant calculated using Equation (35) is given in Table II.

F. DATA ANALYSIS

In view of the fact that the only difference between the three groups of LEDs is the amount and shape of the surface area available for light emittance, the expectation is that the radiation effects observed between the groups would be similar, which they are. In order of decreasing surface area, the groups are A5 (9.7×10^{-4} sq.cm), 3 (8.44×10^{-4} sq.cm), and then 9 (4.95×10^{-4} sq.cm). Keeping in mind that the lifetime damage constant is an "inverse" figure of merit, that is the larger the $\tau_o K$ product, the more susceptible the device is to radiation damage, group rankings from worst to best are: group 9 (2.9×10^{-14} cm^2/e), group A5 (2.6×10^{-14} cm^2/e) and, group 3 (1.4×10^{-14} cm^2/e), where the numbers inside the parenthesis are the average damage constant for

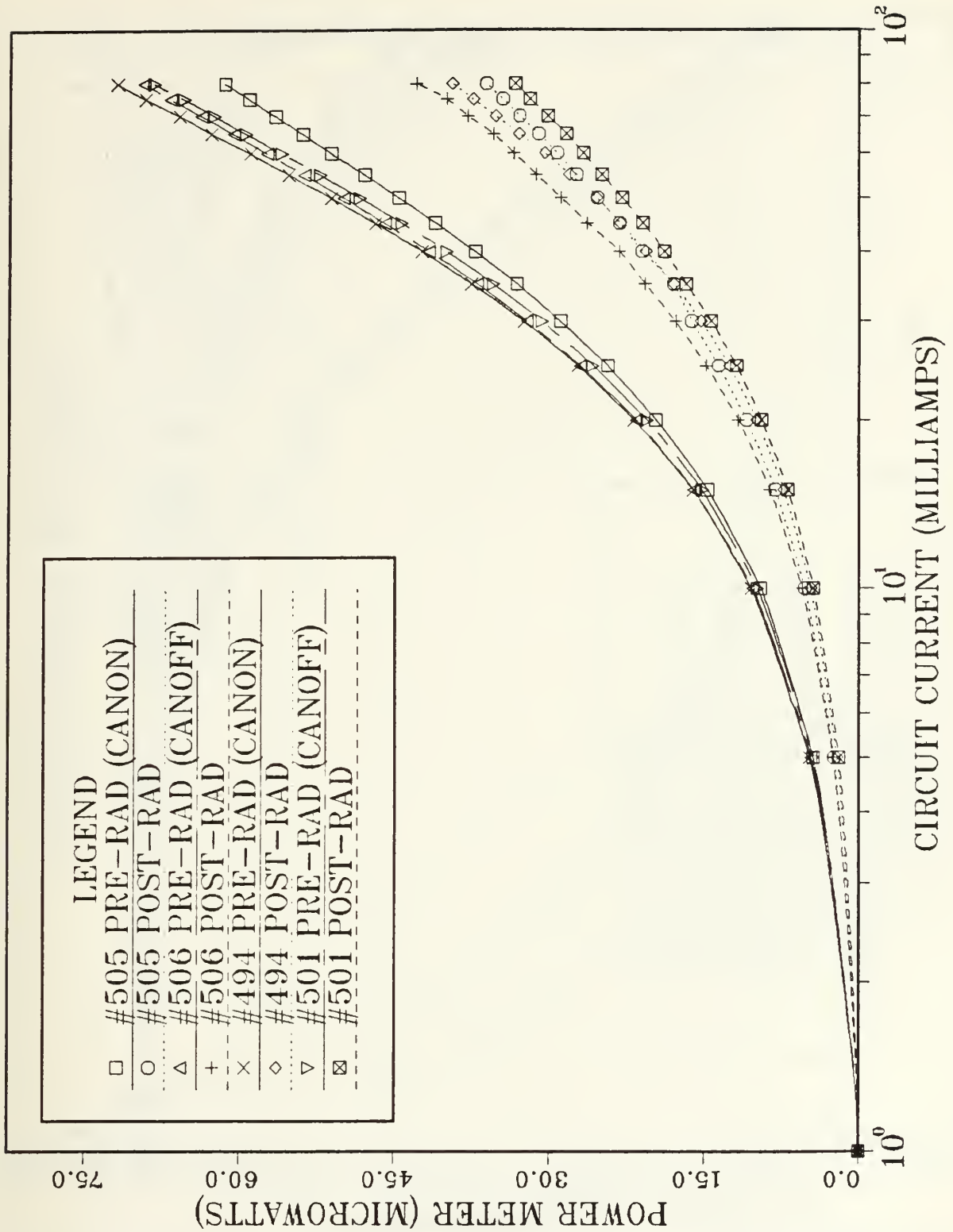

Figure 27. Absolute Light Output versus Current at 0° Offset (— before can-on, ... after can-on —·— before can-off, --- after can-off)

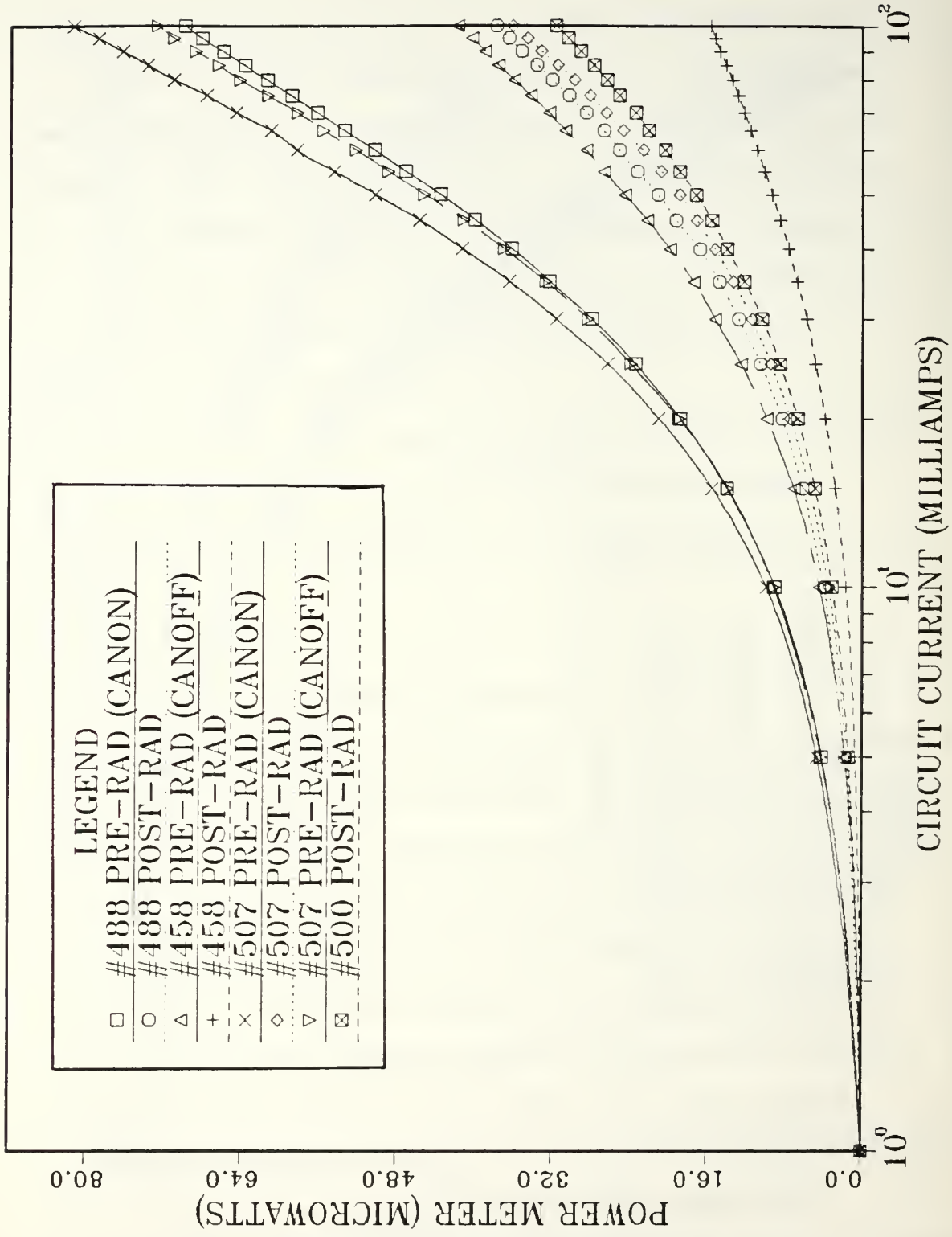

Figure 28. Absolute Light Output versus Current at 45° Offset (— before can-on, ... after can-on —·— before can-off, --- after can-off)

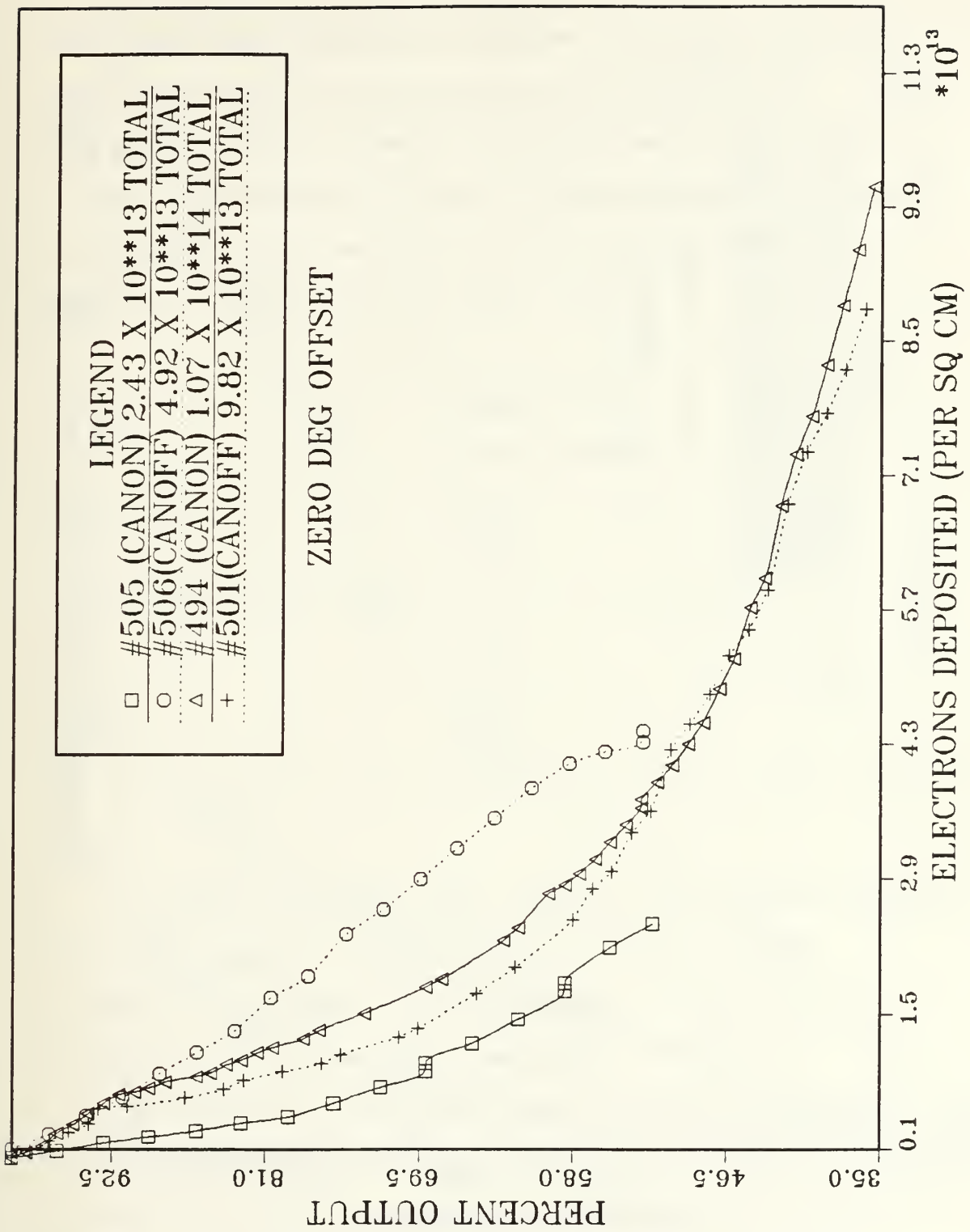

Figure 29. Relative Light Output versus Accumulated Electron Dose at 0° Offset (— can-on, ... can-off)

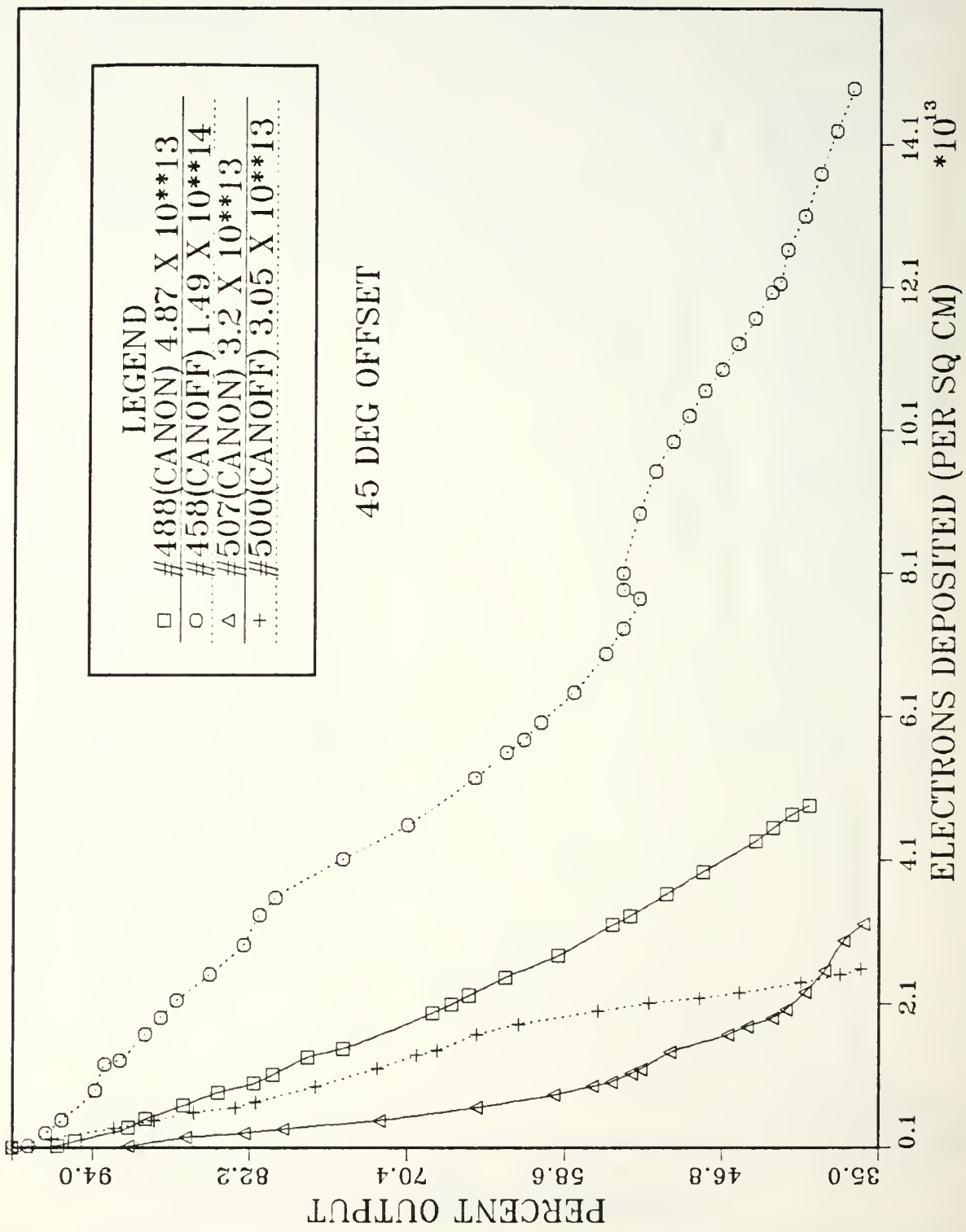

Figure 30. Relative Light Output versus Accumulated Electron Dose at 45° Offset (— can-on, ... can-off)

the group. The differences between the damage constants found are felt not to be statistically significant. Group 9's place as the "softest" device tested is of interest as it was the only one to have a circular area of luminescence. No substantiated reason for this is offered here. These results are summarized in Table III.

TABLE III

DEVICE SUMMARY

group #	area (10^{-4}) (cm^2)	T_0K (10^{-14}) (cm^2/e)
9	4.95	2.9
3	8.44	1.4
A5	9.70	2.6

In comparison with other research, Millea and Aukerman [Ref. 4] reported a damage constant of 2×10^{-15} cm^2/e for GaAs LEDs. This is an order of magnitude harder than found in this research.

The effect of increased current flow and decreased light output intensity at a given forward bias voltage after irradiation, is comparable with the results of previous work. The results are consistent with Barnes' findings [Ref. 2] where, in diffusion controlled devices, radiation induced defects apparently acted as non-radiative recombination

centers which competed for the injected minority carriers. This would explain the increased current after irradiation as the injected carriers being captured by these non-radiative centers would act only to increase the total current through the device, and not the light output intensity.

Results based on the data comparisons between the can-on and can-off device configurations are felt to be inconclusive. Although predictions matched results in the cases of the devices with the can-on having a higher damage constant than the can-offs, and the 45° offset can-ons having the highest of all, the damage trends as viewed in Figures 29 and 30 are considered to be within an acceptable statistical spread and do not show a significant difference between can-on and can-off configurations. In addition, the uncertainty of the position of the device in the beam is of some concern. The possibility exists that the device with the larger damage constant may be due to the device being in the center of the beam while the devices with lesser constants may have resided at the edges of the beam pattern. The SEMs would register the same accumulated fluence for both devices, when in fact there would be a significant difference.

Calculations have indicated that a primary electron from the 30 Mev beam passing through the 2 mill thick nickel-alloy Covar can surrounding the semiconductor chip,

could produce on the order of 1000 secondary electrons. However, these secondary electrons are of a much less energy (on the order of the energy loss that the primary electron undergoes during its' radiative interaction) and do not necessarily follow the path of the primary electron. In addition, it is not known if the secondary electrons have enough energy to cross the distance from the can to the semiconductor chip. If they can make this transition, the question as to if the electrons now have enough energy to induce a defect into the crystal lattice still remains. These additional uncertainties which, are the basis for the inconclusiveness of the results, lead to some recommendations for future research which are offered in Chapter V.

V. CONCLUSIONS AND RECOMMENDATIONS FOR FUTURE WORK

A. CONCLUSIONS

The results of this research into the effects of 30 MeV electron beam irradiation of $GaAs_{.7}P_{.3}$ LEDs indicate that the devices tested are an order of magnitude softer to electron radiation damage than others previously cited in past research. The calculated damage constants are: group 9 (2.92×10^{-14} cm^2/e), group A5 (2.56×10^{-14} cm^2/e), and group 3 (1.37×10^{-14} cm^2/e). Millea and Aukerman [Ref. 4] report a damage constant of 2×10^{-15} cm^2/e for GaAs LEDs, which is an order of magnitude harder to electron radiation than the devices tested in this research. This order of magnitude softness to radiation damage when compared to devices of 10 to 20 years ago is surmised to be due to the fabrication processes employed today. The purity of the crystalline structure is so high that any defect introduced into the lattice produces a noticeable degradation.

The results of the can-on/can-off irradiation runs were felt to be inconclusive. Although the can-on devices at a 45^{o} offset angle had the highest damage constant (5.3×10^{-14} cm^2/e), it is felt that all the results were statistically insignificant.

The results of the beam profile work led to a better estimation of beam area that is 1/3 the size used in previous research done at the NPSAL LINAC. This, in turn, resulted in a factor of three increase in the calculated total fluence the devices were exposed to.

B. RECOMMENDATIONS FOR FUTURE WORK

The concept of controlling the temperature of the devices while taking current, voltage, and light output intensity measurements is considered to be a valid procedure in a effort to reduce a potentially large source of experimental error. However, in future work some consideration might be given to controlling the device's temperature while being irradiated. Since the target chamber is evacuated, the mechanical process of heat removal by the atmosphere is absent. This condition could lead to a rapidly increasing device temperature which could have a detrimental effect on gathering reliable results. A thermal radiation dose can be expressed as

$$D = \Delta T C_p \rho M \qquad (36)$$

where D is the dose in calories, Cp is the specific heat of the material (cal/^{o}K-mole), ρ is the density of the material (gm/cm^3), and M is the mass of the material being irradiated. Using this equation for the largest

fluence applied to my devices, a maximum temperature rise of 25°K is calculated. This is considered significant in view of the data presented in Figure 6. Because of this, it is surmised that some of the damage shown in the relative light output intensity versus fluence plots (Figures 20 through 27 and 29 through 30), could be indicative of thermally induced degradation and not total radiation damage. It is important to note that this effect would not alter the absolute light output intensity. This data was obtained outside of the evacuated target chamber and in a controlled temperature environment.

In view of the unknowns concerning the actions of the secondary electrons as stated at the end of the previous chapter, two recommendations are offered. During irradiation runs, turn the beam off while the device is still under forward bias and observe the annealing rate. There may exist a recognizable difference in annealing rates between the can-off species and the can-on due to the intensified "electron shower" that the Bremsstrahlung process is capable of producing. This could be done at ambient temperature or coupled with the effort to reduce the temperature effects by having the device under some externally controlled temperature. Another technique would be to install an additional SEM before the target. This SEM could monitor the electron beam prior to any interactions with a target. If a significant difference in accumulated charge readings

existed between the two SEMs, radiative loss mechanisms may then be considered as having a significant effect and this could severely change the fluence calculations. The fluence that has been calculated on the basis of readings from the SEM located after the target may have detected electrons that did not originate in the beam. Rather, they could have been produced by the beam passing through the device and undergoing large radiative-type losses. These losses could generate secondary electrons within the device which exit the base and are "counted" by the SEM. Because these additional electrons did not originate within the beam, they could not have interacted with the device under study and should not be counted. Hence, over-estimation of beam fluence might have occurred.

Finally, the importance of characterization of the beam before each irradiation run cannot be stressed enough. Errors in under-estimation of beam fluence of factors of three or more can occur due to an improper estimation of actual beam area.

APPENDIX A

A MATHEMATICAL APPROXIMATION TO THE CROSS-SECTIONAL ELECTRON DENSITY PROFILE FOR THE NPSAL LINAC ELECTRON BEAM

The data collected through the use of the wire target as described in Chapter III can be used to produce a mathematical model to approximate the electron density profile of a cross-section of the beam. This is done in an effort to produce a better estimation for the actual area to be used in fluence calculations. Once this area is known, device placement within the beam then becomes the critical concern. Since the SEM presents a large enough collection area, it will accumulate all the charge that is in the beam. However, the devices that are being irradiated are of smaller dimensions and, therefore, may be placed anywhere within the beam's elliptical area, not necessarily at the center. This would result in different doses for the same fluences indicated by the SEM.

Figure 10 depicts the data obtained through the use of the wire target. If the profile is projected onto a flat surface, the beam would resemble an ellipse with the major axis along the horizontal or X axis. The total beam charge collected by the SEM can be expressed as

$$Q_T = \int\int Q_o F(x) G(y)\, dx dy \tag{37}$$

where Q_T is the total charge, Q_o is the maximum charge in the center of the beam, and F(x),G(y) are functions that will be used to approximate the gaussian type distribution that the plots of Figure 10 resemble. The integral is over the total beam cross-section. To find the fraction of charge passing through an incremental area (dx,dy) of the beam, we integrate Equation (37) or

$$dQ = Q_o F(x)G(y)dxdy \qquad (38)$$

Then, the fluence can be defined as charge (electrons) per unit area (dQ/dxdy) or as a function dependent on the position within the beam times the maximum charge available

$$J(x,y) = dQ/dxdy = Q_o F(x)G(y) \qquad (39)$$

THe average fluence within the beam, if we approximate the beam profile as a rectangle with side of length 2a and 2b is

$$\langle J \rangle \approx Q_T/4ab \qquad (40)$$

Since the curves of Figure 10 are parabolic in nature, the functions F(x) and G(y) can be approximated as

$$F(x) = (1-x^2/a^2) \qquad G(y) = (1-y^2/b^2) \qquad (41)$$

Substituting these into Equation (37) we have

$$Q_T = Q_o\left[\int_{-a}^{+a}\left(1 - \frac{x^2}{a^2}\right)dx \cdot \int_{-b}^{+b}\left(1 - \frac{y^2}{b^2}\right)dy\right] \qquad (42)$$

which can be integrated to give

$$Q_T = Q_o\left[\left(x - \frac{x^3}{3a^2}\right)\Big|_{-a}^{+a}\right]\left[\left(y - \frac{y^3}{3b^2}\right)\Big|_{-b}^{+b}\right] \qquad (43)$$

Substituting in the limits and solving, the solution reduces to

$$Q_T = Q_o \frac{4}{3}a \frac{4}{3}b = \frac{16}{9}Q_o a b \qquad (44)$$

This can be solved for Q_o and the result used in Equation (41) to give an expression for the average fluence within the elliptical beam profile as

$$Q_o = \frac{9}{16}\frac{Q_T}{ab} = \frac{9}{4}\langle J\rangle \qquad (45)$$

The fluence within the beam at any position (x,y) can now be expressed as

$$J(X,Y) = \frac{9}{4}\langle J\rangle F(X)G(Y) = \frac{9}{16}\frac{Q_T}{ab}F(X)G(Y) \qquad (46)$$

Equation (46) expresses the positional dependencies of fluence within the beam and should be used for dose calculations. Ideally then, if the area (dxdy) of the device is known, the beam current can be calculated. In this research however, an approximation was made that the semi-major and semi-minor axes were the length at the 50% height of the curve in Figure 10 (rather than the beam edges as in Equations 40 and 41) and that the fluence was constant across the area. This approximation resulted in using 0.52 cm^2 for the value of the area used in Equation (31). This is approximately 1/3 the area that would have been used, incorrectly, by measuring the spot size on the phosphor screen. Once the fluence was calculated, 90% of this value was used in the damage constant calculations due to the effect of "beam wander" The primary reason for this "beam wander" approximation is that the device placement within the beam was not known to exact detail. As described, a phosphor screen at the top of the target ladder was used for initial beam focusing and placement. This "beam spot" was drawn onto a television screen in the control room used to monitor the target chamber. The device was then raised up into the beam and its' location was judged solely on when the device entered the area as drawn on the screen. Care was

taken when mounting the devices on the ladder to ensure that they were in vertical alignment with the phosphor screen. However it is not known if, through the process of raising the devices into the beam, they become slanted to the beam due to a misalignment of the stepping motor's vertical axis. There is also the question of parallax between the device and the television camera which could lead to further misalignment. For these reasons it was felt that the approximation gave a reasonably acceptable area presentation.

As an example of how much this misalignment could affect the fluence calculations, assume that our device is at position y = 0, x = a/2. The functions that describe the fluence profile from Equation (42) give : g(0) = 1, and f(a/2) = 3/4. Substituting these values into Equation (46) gives the fluence at (a/2, 0): J(x,y) = 27/16<J>. When compared to a maximum value for the fluence as position (0,0) of J = 9/4<J>, we see that a slight error in placement of the device within the beam could lead to an error in fluence calculation of 25%. It is felt that the problem of knowing exact device locations was the largest source of error in this research.

LIST OF REFERENCES

1. Stanley, A. G., "Comparison of Light Emitting Diodes in a Space Radiation Environment", IEEE Trans. Nucl. Sci., NS-17, p. 239, 1970.

2. Barnes, C. E., "Radiation Effects in Electroluminescent Diodes", IEEE Trans. Nucl. Sci., NS-18, p. 322, 1971.

3. Millea, M. F. and Aukerman, L. W., "The Role of Diffusion Current in the Electroluminescence of GaAs Diodes",J. Appl. Phys., vol 5, no 8, p.168, 1964.

4. Millea, M. F. and Aukerman, L. W., "Band-Filling Current in Heavily Doped GaAs Diodes", J. Appl. Phys., vol 36, no 8, p. 2585, 1965.

5. Millea, M. F. and Aukerman, L. W., "The 1.0 and 1.28 eV Emission from GaAs Diodes", J. Appl. Phys., vol 37, no 4, p. 1788, 1966.

6. Millea, M. F. and Aukerman, L. W., "Diffusion Lengths of Electrons and Holes in GaAs", J. Appl. Phys., vol 38, no 2, p. 685, 1967.

7. Nuese, C. J., Schade, H., and Herrick, D., "Efficiency Degradation of $GaAs_{1-x}P_x$ Electroluminescent Diodes Due to High-energy Electron Irradiation", Metallurgical Trans., vol 1, p. 587, 1970.

8. Rose, B. H. and Barnes, C. E., "Proton Damage Effects on Light Emitting Diodes", J. Appl. Phys., vol 53, no 3, p. 1772, 1982.

9. Muller, R. S. and Kamins, T. I., Device Electronics for Integrated Circuits, John Wiley and Sons, 1977.

10. Sze, S. M., Physics of Semiconductor Devices, John Wiley and Sons, 1981.

11. Bergh, A. A. and Dean, P. J., Light Emitting Diodes, Oxford University Press, 1976.

12. Gage, S., Evans, D., Hodapp, M., and Sorensen, H., Optoelectronics Applications Manual, McGraw Hill, 1977.

13. Enge, H. A., Introduction to Nuclear Physics, Addison-Wesley, 1966.

14. Rudie, N. J., Principles and Techniques of Radiation Hardening, Vol. I, Western Periodicals, 1976.

15. Private Communication with Steven J. Hall of Hewlett-Packard, May 1985.

16. Optoelectronic Designer's Catalog, Hewlett-Packard, 1985.

17. Sproull, R. L. and Phillips, W. A., Modern Physics, John Wiley and Sons, 1980.

18. Barnett, M. T. and Cunneen, W. J., Design and Performance of the Electron Linear Accelerator at the U.S. Naval Postgraduate School, Master's Thesis, Naval Postgraduate School, Monterey, California, 1966.

19. Ness, C. Q., Electron Irradiation of Light Emitting Diodes, Master's Thesis, Naval Postgraduate School, Monterey, California, 1984.

INITIAL DISTRIBUTION LIST

		No. Copies
1.	Defense Technical Information Center Cameron Station Alexandria, Virginia 22304-6145	2
2.	Library, Code 0142 Naval Postgraduate School Monterey, California 93943-5100	2
3.	Prof. K. C. Dimiduk, Code 61Dm Department of Physics Naval Postgraduate School Monterey, California 93943-5100	6
4.	Prof. K. Woehler, Code 61Wh Naval Postgraduate School Monterey, California 93943-5100	1
5.	Lt. J. K. Foley Grove Avenue Chicora, Pennsylvania 16025	2
6.	Mr. J. T. Foley Grove Avenue Chicora, Pennsylvania 16025	1
7.	D. Snyder, Code 61 Department of Physics Naval Postgraduate School Monterey, California 93943-5100	1
8.	S. J. Hall Optoelectronics Division Hewlett-Packard Company 640 Page Mill Road Palo Alto, Califonia 94304	1
9.	Prof. J. A. Pidgeon Kiskiminetas Springs School Saltsburg, Pennsylvania 15681	1
10.	Prof. X. K. Maruyama Center Rad. Res. National Bureau of Standards Gaithersburg, Maryland 20899	1